Symmetry-preserving discretization of turbulent flow

Verstappen, R.W.C.P.; Veldman, A.E.P.

Published in:
Journal of computational physics

DOI:
10.1016/S0021-9991(03)00126-8

Publication date:
2003

ACADEMIC PRESS

Available online at www.sciencedirect.com

SCIENCE DIRECT®

Journal of Computational Physics 187 (2003) 343–368

JOURNAL OF COMPUTATIONAL PHYSICS

www.elsevier.com/locate/jcp

Symmetry-preserving discretization of turbulent flow

R.W.C.P. Verstappen *, A.E.P. Veldman

Research Institute for Mathematics and Computing Science, University of Groningen, P.O. Box 800, AV Groningen 9700, The Netherlands

Accepted 11 June 2002

Abstract

We propose to perform turbulent flow simulations in such manner that the difference operators do have the same symmetry properties as the underlying differential operators, i.e., the convective operator is represented by a skew-symmetric coefficient matrix and the diffusive operator is approximated by a symmetric, positive-definite matrix. Mimicking crucial properties of differential operators forms in itself a motivation for discretizing them in a certain manner. We give it a concrete form by noting that a symmetry-preserving discretization of the Navier–Stokes equations is stable on any grid, and conserves the total mass, momentum and kinetic energy (for the latter the physical dissipation is to be turned off, of coarse). Being stable on any grid, the choice of the grid may be based on the required accuracy solely, and the main question becomes: how accurate is a symmetry-preserving discretization? Its accuracy is tested for a turbulent flow in a channel by comparing the results to those of physical experiments and previous numerical studies. The comparison is carried out for a Reynolds number of 5600, which is based on the channel width and the mean bulk velocity (based on the channel half-width and wall shear velocity the Reynolds number becomes 180). The comparison shows that with a fourth-order, symmetry-preserving method a $64 \times 64 \times 32$ grid suffices to perform an accurate numerical simulation.

AMS: 65M06; 76F65; 76M12

Keywords: Higher-order discretization; Nonuniform grid; Conservation; Stability; Turbulent channel flow; Direct numerical simulation

1. Introduction

More than one and a half century ago Claude Navier (1822) and George Stokes (1845) derived an excellent mathematical model for turbulent flow. 'Their' equations state that (in the absence of compressibility) the fluid velocity $\boldsymbol{u}$ and pressure p satisfy

* Corresponding author. Tel.: +31-50-36-33-958; fax: +31-50-36-33-800.
E-mail addresses: verstappen@math.rug.nl (R.W.C.P. Verstappen), veldman@math.rug.nl (A.E.P. Veldman).

0021-9991/03/$ - see front matter
doi:10.1016/S0021-9991(03)00126-8

$$\partial_t \boldsymbol{u} + (\boldsymbol{u}\cdot\nabla)\boldsymbol{u} - \frac{1}{Re}\nabla\cdot\nabla\boldsymbol{u} + \nabla p = \boldsymbol{0}, \quad \nabla\cdot\boldsymbol{u} = \boldsymbol{0}, \tag{1}$$

where the parameter Re denotes the Reynolds number.

Turbulence is basically the combination of nonlinear transport and dissipation of energy. Very crudely put, energy is convected from the main flow into the large eddies, and from them into the next smaller eddies, and so on until it comes within the reach of dissipation. In the absence of external sources (such as body or boundary forces) the rate of change of the *total* energy is neither influenced by convective transport nor by pressure differences; it is solely determined by dissipation. This basic physical property can readily be deduced from the symmetries of the differential operators in the Navier–Stokes equations (1).

The total energy of the flow $(\boldsymbol{u},\boldsymbol{u})$ is defined in terms of the usual scalar product. The evolution can be obtained by differentiating $(\boldsymbol{u},\boldsymbol{u})$ with respect to time and rewriting $\partial_t\boldsymbol{u}$ with the help of Eq. (1). In this way, we get

$$\frac{\mathrm{d}}{\mathrm{d}t}(\boldsymbol{u},\boldsymbol{u}) = -((\boldsymbol{u}\cdot\nabla)\boldsymbol{u},\boldsymbol{u}) - (\boldsymbol{u},(\boldsymbol{u}\cdot\nabla)\boldsymbol{u}) + \frac{1}{Re}((\nabla\cdot\nabla\boldsymbol{u},\boldsymbol{u}) + (\boldsymbol{u},\nabla\cdot\nabla\boldsymbol{u})) - (\nabla p,\boldsymbol{u}) - (\boldsymbol{u},\nabla p).$$

Integrating the linear and trilinear forms in the right-hand side by parts, ignoring any boundary contributions, we obtain: $(\nabla p,\boldsymbol{u}) = -(p,\nabla\cdot\boldsymbol{u})$ and $((\boldsymbol{u}\cdot\nabla)\boldsymbol{v},\boldsymbol{w}) = -(\boldsymbol{v},(\boldsymbol{u}\cdot\nabla)\boldsymbol{w})$, see also [1] for instance. In terms of the differential operators these fundamental properties read

$$(\boldsymbol{u}\cdot\nabla)^* = -(\boldsymbol{u}\cdot\nabla) \quad \text{and} \quad \nabla^* = -\nabla. \tag{2}$$

As a result of these (skew-)symmetries the convective- and pressure-dependent terms cancel and the rate of change of the total energy reduces to

$$\frac{\mathrm{d}}{\mathrm{d}t}(\boldsymbol{u},\boldsymbol{u}) = -\frac{2}{Re}(\nabla\boldsymbol{u},\nabla\boldsymbol{u}) \leqslant 0. \tag{3}$$

In a discrete setting the energy also evolves according to Eq. (3) with $\boldsymbol{u}$ replaced by the discrete velocity, and ∇ by its discrete approximation, provided *the discretizations of the differential operators also possesses the* (*skew-*)*symmetry expressed in Eq.* (2). Under this condition, the energy of any discrete solution is conserved when the flow is inviscid, and decreases in time when dissipation is present. Stated otherwise, *a symmetry-preserving, spatial discretization of the Navier–Stokes equations is unconditionally stable and conservative*. With this in mind, we have developed second- and fourth-order versions, wherein the convective operator $(\boldsymbol{u}\cdot\nabla)$ is approximated by a skew-symmetric discrete operator, and the approximation of the diffusive operator $-\nabla\cdot\nabla$ is symmetric and positive-definite.

1.1. 1D preview

As a preview of things to come we consider the discretization of a first-order derivative in one spatial dimension. In mathematical terms: given three values of a smooth function u, say $u_{i-1} = u(x_{i-1})$, $u_i = u(x_i)$ and $u_{i+1} = u(x_{i+1})$ with $x_{i-1} < x_i < x_{i+1}$, find an approximation of the spatial derivative of u at x_i. Almost any textbook on numerical analysis answers this question by combining Taylor-series expansions of u around $x = x_i$ in such a manner that as many as possible low-order terms cancel. After some algebra this results into the second-order accurate approximation

$$\partial_x u(x_i) \approx \frac{\delta x_i^2 u_{i+1} + \left(\delta x_{i+1}^2 - \delta x_i^2\right)u_i - \delta x_{i+1}^2 u_{i-1}}{\delta x_{i+1}\delta x_i(\delta x_{i+1} + \delta x_i)}, \tag{4}$$

where the grid spacing is denoted by $\delta x_i = x_i - x_{i-1}$. Approximation (4) may also be derived by constructing a parabola through the three given data points and differentiating that parabola at $x = x_i$.

To analyze the conservation and stability properties of the discretization given by (4), we consider the convection–diffusion equation

$$\partial_t u + \bar{u}\partial_x u - \partial_{xx} u/Re = 0, \tag{5}$$

where the convective transport velocity $\bar{u}$ is taken constant, for simplicity. In matrix-vector notation, the spatial discretization of Eq. (5) may be written as

$$\boldsymbol{\Omega}_0 \frac{\mathrm{d}\boldsymbol{u}_h}{\mathrm{d}t} + \boldsymbol{C}_0(\bar{\boldsymbol{u}})\boldsymbol{u}_h + \boldsymbol{D}_0\boldsymbol{u}_h = \boldsymbol{0}, \tag{6}$$

where the discrete velocities u_i constitute the vector $\boldsymbol{u}_h$, the diagonal matrix $\boldsymbol{\Omega}_0$ is built of the spacings of the mesh: $(\boldsymbol{\Omega}_0)_{i,i} = \frac{1}{2}(x_{i+1} - x_{i-1})$; the tridiagonal matrices $\boldsymbol{C}_0(\bar{\boldsymbol{u}})$ and $\boldsymbol{D}_0$ represent the convective and diffusive operator, respectively.

In the absence of diffusion, that is for $\boldsymbol{D}_0 = \boldsymbol{0}$, the energy $\|\boldsymbol{u}_h\|^2 = \boldsymbol{u}_h^* \boldsymbol{\Omega}_0 \boldsymbol{u}_h$ of any solution $\boldsymbol{u}_h$ of the dynamical system (6) is conserved if and only if the right-hand side of

$$\frac{\mathrm{d}}{\mathrm{d}t}\|\boldsymbol{u}_h\|^2 = -\boldsymbol{u}_h^*(\boldsymbol{C}_0(\bar{\boldsymbol{u}}) + \boldsymbol{C}_0^*(\bar{\boldsymbol{u}}))\boldsymbol{u}_h$$

is zero. This conservation property holds (for any $\boldsymbol{u}_h$) if and only if the coefficient matrix $\boldsymbol{C}_0(\bar{\boldsymbol{u}})$ is skew-symmetric,

$$\boldsymbol{C}_0(\bar{\boldsymbol{u}}) + \boldsymbol{C}_0^*(\bar{\boldsymbol{u}}) = \boldsymbol{0}, \tag{7}$$

i.e., the discrete operator $\boldsymbol{C}_0(\bar{\boldsymbol{u}})$ has to inherit the skew-symmetry of the continuous convective derivative $(\boldsymbol{u}\cdot\nabla)$, see Eq. (2).

We see immediately that the discretization given by (4) leads to a coefficient matrix with nonzero diagonal entries (for nonuniform grids). Hence, the traditional approach described by (4) violates the skew-symmetry condition (7). Thus, *if the discretization scheme is constructed to minimize the local truncation error, the skew-symmetry of the convective operator is lost on nonuniform grids, and quantities that are conserved in the continuous formulation, like the kinetic energy, are not conserved in the discrete formulation.*

Not conserved means that the energy is either systematically damped (as in upwind methods) or need be damped explicitly to ensure stability. Anyhow, as artificial dissipation inevitable interferes with the subtle balance between convective transport and physical dissipation, especially at the smallest scales of motion, the essence of turbulence is strained. This forms our main motivation to investigate symmetry-preserving discretization for direct numerical simulation (DNS) of turbulent flow. Rather than concentrating on reducing local truncation error, we select the discretization on physical grounds, and thus attain to

$$\bar{u}\partial_x u(x_i) \approx \bar{u}\frac{u_{i+1} - u_{i-1}}{x_{i+1} - x_{i-1}} = \left(\boldsymbol{\Omega}_0^{-1}\boldsymbol{C}_0(\bar{\boldsymbol{u}})\boldsymbol{u}_h\right)_i. \tag{8}$$

The entries of the tridiagonal matrix $\boldsymbol{C}_0(\bar{\boldsymbol{u}})$ are now given by $\boldsymbol{C}_0(\bar{\boldsymbol{u}})_{i,i-1} = -\frac{1}{2}\bar{u}$, $\boldsymbol{C}_0(\bar{\boldsymbol{u}})_{i,i} = 0$ and $\boldsymbol{C}_0(\bar{\boldsymbol{u}})_{i,i+1} = \frac{1}{2}\bar{u}$. Hence, $\boldsymbol{C}_0(\bar{\boldsymbol{u}})$ satisfies (7).

There are various ways to derive the approximation (8). In a finite-element-setting, for instance, the skew-symmetric formulation follows from a Galerkin projection on the space spanned by the piecewise linear functions ϕ_i with $\phi_i(x_i) = 1$ and $\phi_i(x_j) = 0$ for $i \neq j$, provided that the corresponding mass matrix is lumped on the main diagonal.

The two ways of discretization, given by Eqs. (4) and (8), are illustrated in Fig. 1. Perhaps the symmetry-preserving discretization seems not so accurate at first sight, as the derivative is simply approximated by drawing a straight line from (x_{i-1}, u_{i-1}) to (x_{i+1}, u_{i+1}). The local truncation error is indeed only first-order (unless the grid is almost uniform). Yet, the order of the local truncation error is not decisive. Given

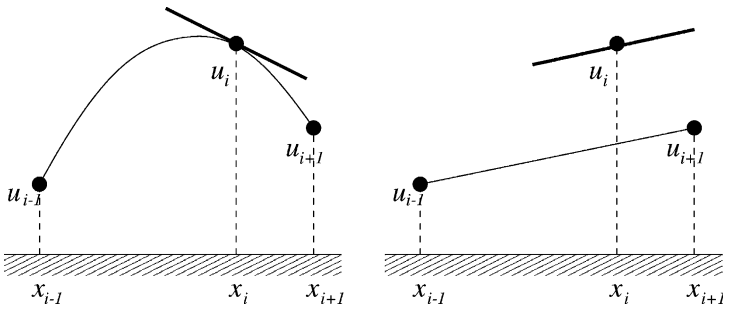

Fig. 1. Two ways of approximating $\partial_x u$. In the left-hand figure the derivative is approximated by means of a Lagrangian interpolation, that is by Eq. (4). In the right-hand figure the symmetry-preserving discretization (8) is applied.

stability, a second-order local truncation error forms a sufficient, but not a necessary, condition for the solution to be second-order, as is emphasized by Manteufel and White [2]. They have rigorously proven that *the approximation* (8) *yields second-order accurate solutions on uniform as well as on nonuniform meshes*.

Diffusion is discretized in the same vein. The resulting coefficient matrix $\boldsymbol{D}_0$ is positive-definite, like the underlying differential operator $-\partial_{xx}$:

$$\boldsymbol{D}_0 = \frac{1}{Re}\boldsymbol{\Delta}_0^*\boldsymbol{\Lambda}_0^{-1}\boldsymbol{\Delta}_0,$$

where the difference matrix $\boldsymbol{\Delta}_0$ is defined by $(\boldsymbol{\Delta}_0\boldsymbol{u}_h)_i = u_i - u_{i-1}$, and the nonzero entries of the diagonal matrix $\boldsymbol{\Lambda}_0$ read $(\boldsymbol{\Lambda}_0)_{i,i} = \delta x_i$. Now, the symmetric part of $\boldsymbol{C}_0(\bar{\boldsymbol{u}}) + \boldsymbol{D}_0$ is only determined by diffusion, and hence is positive-definite. The energy of any solution $\boldsymbol{u}_h$ of the semi-discrete system (6) evolves like in the continuous case; compare Eq. (3) to

$$\frac{\mathrm{d}}{\mathrm{d}t}\left(\boldsymbol{u}_h^*\boldsymbol{\Omega}_0\boldsymbol{u}_h\right) \overset{(6)+(7)}{=} -\boldsymbol{u}_h^*(\boldsymbol{D}_0 + \boldsymbol{D}_0^*)\boldsymbol{u}_h \leqslant 0,$$

where the right-hand side is zero if and only if $\boldsymbol{u}_h$ lies in the null space of $\boldsymbol{D}_0 + \boldsymbol{D}_0^*$. So, in conclusion, since the energy $\|\boldsymbol{u}_h\|^2 = (\boldsymbol{u}_h^*\boldsymbol{\Omega}_0\boldsymbol{u}_h)$ does not increase in time, a stable solution can be obtained on any grid.

Note that the matrix $\boldsymbol{C}_0(\bar{\boldsymbol{u}}) + \boldsymbol{D}_0$ is regular, because all eigenvalues lie in the stable half-plane. This is important for the relationship between the global and local truncation error. In the stationary case, for instance, the global truncation error is equal to the product of the inverse of $\boldsymbol{C}_0(\bar{\boldsymbol{u}}) + \boldsymbol{D}_0$ and the local truncation error. Therefore, a (nearly) singular discrete operator can destroy favorable properties of the local truncation error. Examples of this (for non-symmetry-preserving discretizations!) can be found in [3].

1.2. Higher-order discretization

Higher-order discretization methods are usually more efficient for DNS than low-order discretizations. Therefore, we will next turn Eq. (6) into a fourth-order method. To that end we write down a similar equation on a two times larger control volume

$$\boldsymbol{\Omega}_2\frac{\mathrm{d}\boldsymbol{u}_h}{\mathrm{d}t} + \boldsymbol{C}_2(\bar{\boldsymbol{u}})\boldsymbol{u}_h + \boldsymbol{D}_2\boldsymbol{u}_h = \boldsymbol{0}, \tag{9}$$

where $\boldsymbol{\Omega}_2$ is a diagonal matrix with entries $\frac{1}{2}(x_{i+2} - x_{i-2})$. The convective term is given by $(\boldsymbol{C}_2(\bar{\boldsymbol{u}})\boldsymbol{u}_h)_i = \frac{1}{2}\bar{u}(u_{i+2} - u_{i-2})$ and the diffusive matrix $\boldsymbol{D}_2$ is constructed out of $(\boldsymbol{\Delta}_2\boldsymbol{u}_h)_i = u_{i+1} - u_{i-1}$ and $(\boldsymbol{\Lambda}_2)_{ii} = x_{i+1} - x_{i-1}$.

The leading term in the discretization error can be removed through a Richardson extrapolation from the pair (6)–(9). Since the errors in these expressions are of third order, on a uniform grid this would mean to make a combination $2^3\times$ Eq. (6) minus Eq. (9). On a nonuniform grid one would be tempted to tune the weights, 8 and -1, to the actual mesh sizes, but this breaks the symmetry. Therefore, we take the weights independent of the grid location, and hence equal to the uniform weights. In this way the discretization of the convective derivative becomes $(8\boldsymbol{\Omega}_0-\boldsymbol{\Omega}_2)^{-1}(8\boldsymbol{C}_0-\boldsymbol{C}_2)\boldsymbol{u}_h$. Or, written out per element,

$$\partial_x u(x_i)\approx\frac{-u_{i+2}+8u_{i+1}-8u_{i-1}+u_{i-2}}{-x_{i+2}+8x_{i+1}-8x_{i-1}+x_{i-2}}. \tag{10}$$

Alternatively, this approximation may also be derived by means of the coordinate transformation $x=x(\xi)$, which maps the nonuniform grid in x onto a uniform grid in ξ. Prior to discretization, we rewrite the (partial) derivative of u with respect to x as a quotient of derivatives with respect to ξ

$$\frac{\partial u}{\partial x}=\frac{\partial u}{\partial\xi}\frac{\mathrm{d}\xi}{\mathrm{d}x}=\frac{\partial u}{\partial\xi}\Big/\frac{\mathrm{d}x}{\mathrm{d}\xi}.$$

The two ξ-derivatives in the right-hand side are discretized on the ξ-grid, which has a uniform spacing denoted by h. Neglecting fourth-order terms in

$$\frac{\partial u}{\partial\xi}(\xi_i)=\frac{-u_{i+2}+8u_{i+1}-8u_{i-1}+u_{i-2}}{12h}+\mathrm{O}(h^4)$$

and

$$\frac{\mathrm{d}x}{\mathrm{d}\xi}(\xi_i)=\frac{-x_{i+2}+8x_{i+1}-8x_{i-1}+x_{i-2}}{12h}+\mathrm{O}(h^4),$$

gives the approximation (10). This alternative derivation illustrates the fourth-order accuracy of the skew-symmetric discretization (10) on nonuniform grids. Therewith it founds our choice for taking constant weights in the Richardson extrapolation. On uniform grids we obtain, of course, the usual fourth-order method, but on nonuniform grids the method differs! For practical experiences with the second-order, symmetry-preserving discretization method we refer to [3]. Experiences with the fourth-order, symmetry-preserving discretization (10) can be found in Section 4.1.

It goes without saying that both stability and conservation properties have a long standing in the analysis of discretization methods. Recently, conservation properties of numerical schemes for the (incompressible) Navier–Stokes equations are also pursued by other researchers, in particular at Stanford University [4–6], at CERFACS [7] and at Delft University [8,9].

Morinishi et al. [4] have considered a family of higher-order discretization schemes for incompressible flow that almost/fully conserve mass, momentum and kinetic energy. On a uniform grid, their fully conservative, finite-difference approximation of the convective terms in the Navier–Stokes equations (given by Eq. (101) in [4]) is identical to our fourth-order discretization. The current issue is how to generalize this fully conservative, fourth-order scheme to nonuniform grids while preserving the conservation properties as well as the (formal) accuracy. At this point the approaches diverge. On nonuniform grids, Morinishi et al. prefer a nonconservative scheme (referred to as *Adv.-S4-S* in their paper) that preserves the formal, fourth-order accuracy. Vasilyev [5] also adopts this starting-point. He generalizes the schemes of Morinishi et al. to nonuniform meshes while maintaining the formal, fourth-order accuracy (by means of a mapping technique). However, the conservation properties are sacrificed. Vasilyev's schemes do not simultaneously conserve momentum and energy. Depending on the choice made for the discretization of the convective term, conservation of either momentum or energy in addition to mass is achieved in [5]. As explained in the

1D preview, we do not strive for a minimal local truncation error, but aim to preserve the conservation properties, by preserving the symmetry of the underlying differential operators.

Nicoud [6] concerns a low-Mach number approximation for the Navier–Stokes equations where the energy conservation is violated unless an approximate state equation is used. Ducros et al. [7] deal with compressible flow. They extend Jameson's second-order finite volume method [10] to a family of higher-order 'skew-symmetric-like' centered schemes. At Delft University [8,9], a variant of our symmetry-preserving discretization for collocated grids has been developed. Last, but not least, although not yet applied to the Navier–Stokes equations, we like to mention both the procedure for designing by rote finite-difference schemes that inherit energy conservation from conservative p.d.e.'s by Furihata [11] and the mimetic method by Hyman et al. [12–14] for constructing finite-difference approximations that retain/mimic the main properties of the continuum problem to be solved.

The paper is organized as follows. The symmetry-preserving discretization method is outlined in Section 2. We describe a second- and a fourth-order version, discuss their conservation and stability properties, and end Section 2 with the incorporation of boundary conditions. Because we want to apply our method to turbulent flow, we need a time-integration technique too. The one-leg method that we have used is briefly sketched in Section 3. Having set the method, the accuracy is tested for two examples in Section 4. To start, we consider a one-dimensional convection–diffusion equation of which an exact solution is known. After that, the accuracy is illustrated for a fully developed, turbulent channel flow (at a Reynolds number of 5600, based on the channel width and the mean bulk velocity; or 180, based on the channel half-width and wall shear velocity) by comparing the results to those of physical experiments and previous numerical studies. The symmetry-preserving discretization method has also been applied to more complex turbulent flows with heat transfer. For results thereof, we refer to a forthcoming, companion paper [15]. Results of complex flow simulations with a predecessor of the present method can be found in [16,17].

2. Symmetry-preserving spatial discretization

In the introductory section, we saw that conservation properties and stability are directly related to the symmetry of the underlying differential operators. In this section, we will work this out for the incompressible Navier–Stokes equations, where we will restrict ourselves to two spatial dimensions to limit the length of the presentation; the extension to 3D is straightforward.

2.1. Basic, second-order method

On a uniform grid the traditional aim, minimize the local truncation error, need not break the symmetries of the convective and diffusive operators in the Navier–Stokes equations. The well-known scheme of Harlow and Welsh [18] forms an example of this. We will generalize Harlow and Welsh's scheme to nonuniform grids in such a manner that the symmetry remains unbroken. The notation used subsequently in this section is the same as in [18]. The setting is illustrated in Fig. 2.

2.1.1. Convective discretization

To prepare for the skew-symmetric, finite-volume discretization of the convective derivative, we recall the transport theorem: for any function f of $\boldsymbol{x}$ and t, we have

$$\frac{\mathrm{d}}{\mathrm{d}t}\int_{\Omega} f\,\mathrm{d}V = \int_{\Omega}\frac{\partial f}{\partial t}\,\mathrm{d}V + \int_{\partial\Omega} f\boldsymbol{u}\cdot\boldsymbol{n}\,\mathrm{d}S, \tag{11}$$

where Ω is an arbitrary part of the fluid at a particular instant of the time t. The unit vector $\boldsymbol{n}$ denotes the outward normal on the surface $\partial\Omega$ of Ω. The (scalar or vector) function f in (11) can have several meanings

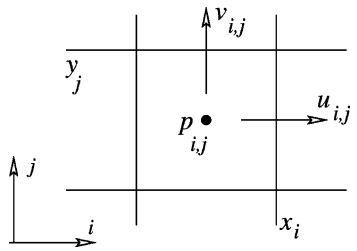

Fig. 2. The location of the discrete velocities.

depending on what is transported. Taking f equal to the mass density of the fluid gives the law of conservation of mass. For an incompressible fluid, it states that the net mass flux through the faces of any control volume $\Omega_{i,j} = [x_{i-1}, x_i] \times [y_{j-1}, y_j]$ is zero,

$$\bar{u}_{i,j} + \bar{v}_{i,j} - \bar{u}_{i-1,j} - \bar{v}_{i,j-1} = 0, \tag{12}$$

where $\bar{u}_{i,j}$ denotes the mass flux through the face $y = y_j$ of the grid cell $\Omega_{i,j}$ and $\bar{v}_{i,j}$ stands for the mass flux through the grid face $x = x_i$:

$$\bar{u}_{i,j} = \int_{y_{j-1}}^{y_j} u(x_i, y, t)\,\mathrm{d}y \quad \text{and} \quad \bar{v}_{i,j} = \int_{x_{i-1}}^{x_i} v(x, y_j, t)\,\mathrm{d}x. \tag{13}$$

The combination (12) and (13) does not contain a discretization error, since the integrals in (13) have not yet been discretized. We postpone their discretization until later in this section. Until then we view the velocities $(u_{i,j}, v_{i,j})$ as the unknowns and the mass fluxes $(\bar{u}_{i,j}, \bar{v}_{i,j})$ as being given such that the constraint (12) holds.

The transport of momentum of a region Ω in an incompressible fluid is obtained if f in Eq. (11) is replaced by the velocity. As mass and momentum are transported at equal velocity, the mass fluxes are used to discretize the transport velocity of momentum. Thus, the (spatial) discretization of the transport of the u-component of momentum of a region $\Omega_{i+1/2,j} = [x_{i-1/2}, x_{i+1/2}] \times [y_{j-1}, y_j]$ becomes (see also Fig. 3)

$$|\Omega_{i+1/2,j}| \frac{\mathrm{d}u_{i,j}}{\mathrm{d}t} + \bar{u}_{i+1/2,j} u_{i+1/2,j} + \bar{v}_{i+1/2,j} u_{i,j+1/2} - \bar{u}_{i-1/2,j} u_{i-1/2,j} - \bar{v}_{i+1/2,j-1} u_{i,j-1/2}. \tag{14}$$

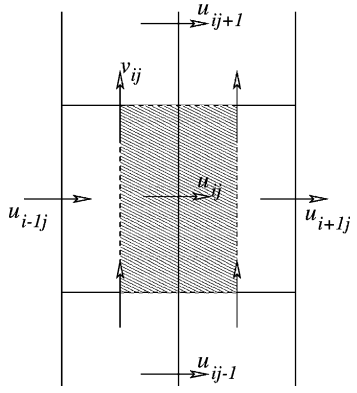

Fig. 3. The control volume $\Omega_{i+1/2,j}$ for the discrete, horizontal velocity $u_{i,j}$.

The first term in (14) represents the discretization of the volume integral in the right-hand side of Eq. (11); the other terms form the approximation of the surface integral in (11) with $f = u$. The non-integer indices in (14) refer to the faces of $\Omega_{i+1/2,j}$. For example, $u_{i-1/2,j}$ stands for the u-velocity at the interface of $\Omega_{i-1/2,j}$ and $\Omega_{i+1/2,j}$. The velocity at a control face is approximated by the average of the velocity at both sides of it:

$$u_{i+1/2,j} = \frac{1}{2}(u_{i+1,j} + u_{i,j}) \quad \text{and} \quad u_{i,j+1/2} = \frac{1}{2}(u_{i,j+1} + u_{i,j}). \tag{15}$$

Substituting the interpolation rule (15) into the discretization (14) gives

$$|\Omega_{i+1/2,j}|\frac{\mathrm{d}u_{i,j}}{\mathrm{d}t} + \frac{1}{2}(\bar{u}_{i+1/2,j} + \bar{v}_{i+1/2,j} - \bar{u}_{i-1/2,j} - \bar{v}_{i+1/2,j-1})u_{i,j} + \frac{1}{2}\bar{u}_{i+1/2,j}u_{i+1,j} - \frac{1}{2}\bar{u}_{i-1/2,j}u_{i-1,j} + \frac{1}{2}\bar{v}_{i+1/2,j}u_{i,j+1} - \frac{1}{2}\bar{v}_{i+1/2,j-1}u_{i,j-1}. \tag{16}$$

In addition to the set of equations for the u-component of the velocity, there is an analogous set for the v-component:

$$|\Omega_{i,j+1/2}|\frac{\mathrm{d}v_{i,j}}{\mathrm{d}t} + \frac{1}{2}(\bar{v}_{i,j+1/2} + \bar{u}_{i,j+1/2} - \bar{v}_{i,j-1/2} - \bar{u}_{i-1,j+1/2})v_{i,j} + \frac{1}{2}\bar{v}_{i,j+1/2}v_{i,j+1} - \frac{1}{2}\bar{v}_{i,j-1/2}v_{i,j-1} + \frac{1}{2}\bar{u}_{i,j+1/2}v_{i+1,j} - \frac{1}{2}\bar{u}_{i-1,j+1/2}v_{i-1,j}. \tag{17}$$

We conceive Eqs. (16) and (17) as expressions for the velocities, where the mass fluxes $\bar{u}$ and $\bar{v}$ form the coefficients. Thus, in the absence of any (in- or external) forces, we can write the (semi-)discretization of the transport equation in matrix-vector notation as

$$\boldsymbol{\Omega}_1\frac{\mathrm{d}\boldsymbol{u}_h}{\mathrm{d}t} + \boldsymbol{C}_1(\bar{\boldsymbol{u}})\boldsymbol{u}_h = \boldsymbol{0}, \tag{18}$$

where $\boldsymbol{u}_h$ denotes the discrete velocity-vector (which consists of both the $u_{i,j}$'s and $v_{i,j}$'s), $\boldsymbol{\Omega}_1$ is a (positive-definite) diagonal matrix representing the sizes of the control volumes $|\Omega_{i+1/2,j}|$ and $|\Omega_{i,j+1/2}|$, whereas $\boldsymbol{C}_1(\bar{\boldsymbol{u}})$ is built from the flux contributions through the control faces, i.e., $\boldsymbol{C}_1$ depends on the mass fluxes $\bar{u}$ and $\bar{v}$ at the control faces.

From a physical point of view, Eq. (18) must conserve the discrete energy $\boldsymbol{u}_h^*\boldsymbol{\Omega}_1\boldsymbol{u}_h$ in time. As explained in the introductory section, this conservation property is directly related to the skew-symmetry of the convective operator: the energy of any solution $\boldsymbol{u}_h$ of Eq. (18) is conserved,

$$\frac{\mathrm{d}}{\mathrm{d}t}\left(\boldsymbol{u}_h^*\boldsymbol{\Omega}_1\boldsymbol{u}_h\right) = -\boldsymbol{u}_h^*(\boldsymbol{C}_1(\bar{\boldsymbol{u}}) + \boldsymbol{C}_1^*(\bar{\boldsymbol{u}}))\boldsymbol{u}_h = 0,$$

if and only if the coefficient matrix $\boldsymbol{C}_1(\bar{\boldsymbol{u}})$ is skew-symmetric:

$$\boldsymbol{C}_1(\bar{\boldsymbol{u}}) + \boldsymbol{C}_1^*(\bar{\boldsymbol{u}}) = \boldsymbol{0}. \tag{19}$$

2.1.2. Skew-symmetry of convective derivative

Condition (19) is verified in two steps. To start, we consider the off-diagonal elements. The matrix $\boldsymbol{C}_1(\bar{\boldsymbol{u}}) - \mathrm{diag}(\boldsymbol{C}_1(\bar{\boldsymbol{u}}))$ is skew-symmetric if and only if the weights in the interpolations of the discrete velocities are taken constant. To illustrate this, we consider the general interpolation rule

$$u_{i+1/2,j} = (1 - \omega_{i,j})u_{i+1,j} + \omega_{i,j}u_{i,j},$$

instead of (15), where the coefficient $\omega_{i,j}$ may depend on the local mesh sizes. By substituting this interpolation rule into Eq. (14) we see that the coefficient of $u_{i+1,j}$ becomes $(1-\omega_{i,j})\bar{u}_{i+1/2,j}$, while the term $u_{i-1/2,j}\bar{u}_{i-1/2,j}$ in (14) with i replaced by $i+1$ yields the coefficient $-\omega_{i,j}\bar{u}_{i+1/2,j}$ for $u_{i,j}$. For skew-symmetry, these two coefficients should be of opposite sign. Ergo, we should have

$$(1-\omega_{i,j})\bar{u}_{i+1/2,j} = \omega_{i,j}\bar{u}_{i+1/2,j},$$

for all mass fluxes $\bar{u}_{i+1/2,j}$. This can only be achieved when the weight $\omega_{i,j}$ is taken equal to the uniform weight $\omega_{i,j} = 1/2$, hence independent of the grid location. Therefore we take constant weights in Eq. (15), also on nonuniform grids. Stated from a physical point of view the convective flux through the common interface between two neighboring control volumes has to be computed independent of the control volume in which it is considered.

Next, we consider the diagonal of $\boldsymbol{C}_1$. In the notation above, we have suppressed the argument $\bar{\boldsymbol{u}}$ of $\boldsymbol{C}_1$, because $\boldsymbol{C}_1 - \mathrm{diag}(\boldsymbol{C}_1)$ is skew-symmetric for all $\bar{\boldsymbol{u}}$. The interpolation rule for the mass fluxes $\bar{u}$ and $\bar{v}$ through the faces of the control volumes is determined by the requirement that the diagonal of $\boldsymbol{C}_1$ has to be zero. The diagonal coefficient in (16) is given by

$$\frac{1}{2}(\bar{u}_{i+1/2,j} + \bar{v}_{i+1/2,j} - \bar{u}_{i-1/2,j} - \bar{v}_{i+1/2,j-1}). \tag{20}$$

This coefficient equals the average of the net mass fluxes through the faces of the grid volumes $\Omega_{i,j}$ and $\Omega_{i+1,j}$—hence equals zero according to Eq. (12)—if the interpolation of the mass fluxes to the faces of a u-cell is performed with constant weights:

$$\bar{u}_{i+1/2,j} = \frac{1}{2}(\bar{u}_{i+1,j} + \bar{u}_{i,j}) \quad \text{and} \quad \bar{v}_{i+1/2,j} = \frac{1}{2}(\bar{v}_{i+1,j} + \bar{v}_{i,j}). \tag{21}$$

It goes without saying that this interpolation rule is also applied in the j-direction, so that the diagonal coefficient in (17) is zero too. In summary, the coefficient matrix $\boldsymbol{C}_1$ is skew-symmetric if Eq. (12) holds, and if the discrete velocities $\boldsymbol{u}_h$ and fluxes $\bar{\boldsymbol{u}}$ are interpolated to the surfaces of control cells with weights $\frac{1}{2}$, as in Eqs. (15) and (21).

2.1.3. The discrete divergence and gradient

Obviously, the mass flux $\bar{\boldsymbol{u}}$ need be expressed in terms of the discrete velocity vector $\boldsymbol{u}_h$ to close the system of equations (18). The coefficient matrix $\boldsymbol{C}_1(\bar{\boldsymbol{u}})$ becomes a function of the discrete velocity $\boldsymbol{u}_h$ then. We will make liberal use of its name, and denote the resulting coefficient matrix by $\boldsymbol{C}_1(\boldsymbol{u}_h) = \boldsymbol{C}_1(\bar{\boldsymbol{u}}(\boldsymbol{u}_h))$. The matrix $\boldsymbol{C}_1(\boldsymbol{u}_h)$ is skew-symmetric for any relation between $\bar{\boldsymbol{u}}$ and $\boldsymbol{u}_h$. We relate the mass fluxes $\bar{\boldsymbol{u}}$ to the discrete velocity $\boldsymbol{u}_h$ by means the mid-point rule:

$$\bar{u}_{i,j} = (y_j - y_{j-1})u_{i,j} \quad \text{and} \quad \bar{v}_{i,j} = (x_i - x_{i-1})v_{i,j}. \tag{22}$$

Substituting these approximations into Eq. (12) gives the discrete continuity constraint, which confines the discrete velocity to $\boldsymbol{M}_1\boldsymbol{u}_h = \text{given}$, where the right-hand side consists of prescribed mass fluxes through the boundaries of the computational domain. To keep the expressions simple, we take the right-hand side equal to zero,

$$\boldsymbol{M}_1\boldsymbol{u}_h = \boldsymbol{0}, \tag{23}$$

i.e., we restrict ourselves to impervious or periodical boundaries. Note that the coefficient matrix $\boldsymbol{M}_1$ represents the discretization of the divergence operator, integrated over the control volumes, see Eqs. (12) and (13).

The pressure gradient in the Navier–Stokes equations (1) is discretized with the help of the symmetry relation (2). According to Eq. (2) the continuous gradient operator equals the negative of the transpose of

the divergence, i.e., any velocity field $\boldsymbol{u}$ and pressure p satisfy $(\nabla p, \boldsymbol{u}) = -(p, \nabla \cdot \boldsymbol{u})$. Now, let $\boldsymbol{p}_h$ denote the discrete pressure and $\boldsymbol{G}_1\boldsymbol{p}_h$ the discrete pressure gradient. Then, the above relation holds also for the discretization, that is

$$(\boldsymbol{G}_1\boldsymbol{p}_h)^*\boldsymbol{\Omega}_1\boldsymbol{u}_h = \boldsymbol{p}_h^*\boldsymbol{G}_1^*\boldsymbol{\Omega}_1\boldsymbol{u}_h = -\boldsymbol{p}_h^*\boldsymbol{M}_1\boldsymbol{u}_h,$$

if the gradient operator is approximated by

$$\boldsymbol{G}_1 = -\boldsymbol{\Omega}_1^{-1}\boldsymbol{M}_1^*. \tag{24}$$

Note that the gradient matrix, describing the integration of the pressure gradient over the control volumes $\boldsymbol{\Omega}_1$, is given by $-\boldsymbol{M}_1^*$. Because the discrete gradient inherits also the boundary conditions from the discrete divergence, we need not specify boundary conditions for the pressure. As usual, see e.g. [18], we compute the pressure from a Poisson equation, where the Laplacian is approximated by the matrix $-\boldsymbol{M}_1\boldsymbol{\Omega}_1^{-1}\boldsymbol{M}_1^*$, which is symmetric and negative-definite, just like the continuous Laplace operator.

2.1.4. Diffusive discretization

The method for discretizing the Laplacian in the Poisson equation for the pressure is also applied to discretize the diffusive term in the Navier–Stokes equations. In short, the diffusive operator is viewed as the product of two first-order differential operators, a divergence and a gradient. The divergence is discretized and the discrete gradient becomes the transpose of the discrete divergence (multiplied by a diagonal scaling). This construction leads to a symmetric, positive-definite, approximation of the diffusive operator $-\nabla \cdot \nabla$.

Unfortunately, we cannot re-use the approximation $\boldsymbol{M}_1\boldsymbol{\Omega}_1^{-1}\boldsymbol{M}_1^*$, since the grid is staggered. Due to the staggering of the grid the control volumes for the velocity components $u_{i,j}$ and $v_{i,j}$ differ from the control volumes $\Omega_{i,j}$ on which coefficient matrix $\boldsymbol{M}_1$ is based. Therefore, we have to introduce the matrices $\boldsymbol{M}_1^u$ and $\boldsymbol{M}_1^v$. They stand for the discrete integration of the divergence over the control volumes for u and v, respectively. For example, the diffusive flux through the faces of the control volume $\Omega_{i+1/2,j}$ of $u_{i,j}$ reads

$$\bar{\phi}_{i+1/2,j} - \bar{\phi}_{i-1/2,j} + \bar{\psi}_{i,j} - \bar{\psi}_{i,j-1},$$

where $\phi = \partial_x u/Re$ and $\psi = \partial_y u/Re$. The surface integrals (denoted by an overbar) are approximated according to

$$\bar{\phi}_{i+1/2,j} = (y_j - y_{j-1})\phi_{i+1/2,j} \quad \text{and} \quad \bar{\psi}_{i,j} = (x_{i+1/2} - x_{i-1/2})\psi_{i,j}.$$

In matrix-vector notation, the diffusive flux through the faces of u-cells is given by $\boldsymbol{M}_1^u\phi_h$, where the vector ϕ_h consists of the $\phi_{i+1/2,j}$'s and $\psi_{i,j}$'s. The gradient operator relating ϕ and ψ to the velocity component u is discretized by $-(\boldsymbol{\Omega}_1^u)^{-1}(\boldsymbol{M}_1^u)^*$, where the entries of the diagonal matrix $\boldsymbol{\Omega}_1^u$ are given by $|\Omega_{i,j}|$ and $|\Omega_{i+1/2,j+1/2}|$. In this way we obtain

$$\phi_{i+1/2,j} = \frac{1}{Re}\,\frac{u_{i+1,j} - u_{i,j}}{x_{i+1} - x_i} \quad \text{and} \quad \psi_{i,j} = \frac{1}{Re}\,\frac{u_{i,j+1} - u_{i,j}}{y_{j+1/2} - y_{j-1/2}}.$$

The diffusive flux through v-cells is approximated similarly. Thus, the discretization of the diffusive term in the Navier–Stokes equations becomes $\boldsymbol{\Omega}_1^{-1}\boldsymbol{D}_1\boldsymbol{u}_h$, where the symmetric, positive-definite coefficient matrix $\boldsymbol{D}_1$ is given by

$$\boldsymbol{D}_1 = \frac{1}{Re}\boldsymbol{\Delta}_1^*\boldsymbol{\Lambda}_1^{-1}\boldsymbol{\Delta}_1 \tag{25}$$

with $\boldsymbol{\Delta}_1^* = \mathrm{diag}(\boldsymbol{M}_1^u, \boldsymbol{M}_1^v)$ and $\boldsymbol{\Lambda}_1 = \mathrm{diag}(\boldsymbol{\Omega}_1^u, \boldsymbol{\Omega}_1^v)$.

2.1.5. Discrete Navier–Stokes equations

By adding viscous and pressure forces to the discrete transport equation (18), we obtain the following semi-discrete representation of the incompressible Navier–Stokes equations

$$\boldsymbol{\Omega}_1 \frac{\mathrm{d}\boldsymbol{u}_h}{\mathrm{d}t} + \boldsymbol{C}_1(\boldsymbol{u}_h)\boldsymbol{u}_h + \boldsymbol{D}_1\boldsymbol{u}_h - \boldsymbol{M}_1^*\boldsymbol{p}_h = \boldsymbol{0}, \quad \boldsymbol{M}_1\boldsymbol{u}_h = \boldsymbol{0}. \tag{26}$$

In detail, the evolution of the discrete velocity $u_{i,j}$ reads

$$\delta x_{i+1/2}\delta y_j \frac{\mathrm{d}u_{i,j}}{\mathrm{d}t} + \frac{1}{4}(\delta y_j u_{i,j} + \delta y_j u_{i+1,j})u_{i+1,j} - \frac{1}{4}(\delta y_j u_{i,j} + \delta y_j u_{i-1,j})u_{i-1,j} + \frac{1}{4}(\delta x_i v_{i,j} + \delta x_{i+1} v_{i+1,j})u_{i,j+1}$$

$$- \frac{1}{4}(\delta x_i v_{i,j-1} + \delta x_{i+1} v_{i+1,j-1})u_{i,j-1} - (\bar{\phi}_{i+1/2,j} - \bar{\phi}_{i-1/2,j} + \bar{\psi}_{i,j} - \bar{\psi}_{i,j-1}) + \delta y_j p_{i+1,j} - \delta y_j p_{i,j} = 0,$$

where $\delta x_i = x_i - x_{i-1}$, $\delta y_j = y_j - y_{j-1}$, and $\delta x_{i+1/2} = \frac{1}{2}(\delta x_i + \delta x_{i+1})$, see also Fig. 3 for notations.

As will be shown in the next section, this spatial discretization conserves energy (in the absence of diffusion) as well as mass and momentum.

2.2. Conservation properties and stability

Global conservation laws invoke integrals over the flow domain. These integrals become scalar products when the flow is discretized. The change of the total mass of the flow, for example, is discretized as the scalar product of the constant vector $\boldsymbol{1}$ (where the dimension equals the number of grid cells) and the discrete mass flux $\boldsymbol{M}_1\boldsymbol{u}_h$. Since this scalar product is zero (because $\boldsymbol{M}_1\boldsymbol{u}_h = \boldsymbol{0}$) the total mass is (trivially) conserved.

The total amount of momentum is obtained by taking the scalar product of the velocity vector $\boldsymbol{u}_h$ with the vector $\boldsymbol{\Omega}_1\boldsymbol{1}$ (where the constant vector now has as many entries as there are control volumes for the discrete velocity components $u_{i,j}$ and $v_{i,j}$). The evolution of the total amount of momentum follows straightforwardly from Eq. (26):

$$\frac{\mathrm{d}}{\mathrm{d}t}(\boldsymbol{1}^*\boldsymbol{\Omega}_1\boldsymbol{u}_h) = -\boldsymbol{1}^*(\boldsymbol{C}_1(\boldsymbol{u}_h) + \boldsymbol{D}_1)\boldsymbol{u}_h + \boldsymbol{1}^*\boldsymbol{M}_1^*\boldsymbol{p}_h.$$

Hence, momentum is conserved provided $(\boldsymbol{C}_1(\boldsymbol{u}_h) + \boldsymbol{D}_1)^*\boldsymbol{1} = \boldsymbol{0}$ and the law of conservation of mass is consistently discretized, that is $\boldsymbol{M}_1\boldsymbol{1} = \boldsymbol{0}$. The former condition may be split into two conditions, one for the convective discretization, $\boldsymbol{C}_1^*(\boldsymbol{u}_h)\boldsymbol{1} = \boldsymbol{0}$, and one for the diffusive discretization, $\boldsymbol{D}_1^*\boldsymbol{1} = \boldsymbol{0}$. Moreover we can leave the *'s away, $\boldsymbol{C}_1(\boldsymbol{u}_h)\boldsymbol{1} = \boldsymbol{0}$ and $\boldsymbol{D}_1\boldsymbol{1} = \boldsymbol{0}$, since the convective matrix $\boldsymbol{C}_1(\boldsymbol{u}_h)$ is skew-symmetric and diffusive matrix $\boldsymbol{D}_1$ is symmetric. So it suffices to verify that the constant vector lies in the null space of the approximate, convective and diffusive operators. The row-sums of $\boldsymbol{D}_1$ are zero by construction. Those of $\boldsymbol{C}_1(\boldsymbol{u}_h)$ can be worked out from Eqs. (14) and (15). Each row-sum of the convective matrix $\boldsymbol{C}_1(\boldsymbol{u}_h)$ is equal to two times the corresponding diagonal element, and thus zero, since $\boldsymbol{C}_1(\boldsymbol{u}_h)$ is skew-symmetric.

The discretization is set up such that the evolution of the (kinetic) energy $\boldsymbol{u}_h^*\boldsymbol{\Omega}_1\boldsymbol{u}_h$ of any solution of Eq. (26) is governed by

$$\frac{\mathrm{d}}{\mathrm{d}t}\left(\boldsymbol{u}_h^*\boldsymbol{\Omega}_1\boldsymbol{u}_h\right) = -\boldsymbol{u}_h^*\left(\boldsymbol{C}_1(\boldsymbol{u}_h) + \boldsymbol{C}_1^*(\boldsymbol{u}_h)\right)\boldsymbol{u}_h - \boldsymbol{u}_h^*\left(\boldsymbol{D}_1 + \boldsymbol{D}_1^*\right)\boldsymbol{u}_h + \boldsymbol{u}_h^*\left(\boldsymbol{M}_1^*\boldsymbol{p}_h\right) + \left(\boldsymbol{M}_1^*\boldsymbol{p}_h\right)^*\boldsymbol{u}_h$$

$$\overset{(19)}{=} -\boldsymbol{u}_h^*\left(\boldsymbol{D}_1 + \boldsymbol{D}_1^*\right)\boldsymbol{u}_h \leqslant 0,$$

where the right-hand side is negative for all $\boldsymbol{u}_h$'s, except those in the null space of $\boldsymbol{D}_1 + \boldsymbol{D}_1^*$. The convective term cancels because $\boldsymbol{C}_1(\boldsymbol{u}_h)$ is skew-symmetric; the pressure terms cancel (hence, cannot unstabilize the spatial discretization) because the discrete pressure gradient is related to the transpose of $\boldsymbol{M}_1$, see Eq. (24).

So, in conclusion, for inviscid flow the energy is conserved, whereas for viscous flow the energy $\|\boldsymbol{u}_h\|^2 = \boldsymbol{u}_h^* \boldsymbol{\Omega}_1 \boldsymbol{u}_h$ does not increases in time. This implies that the semi-discrete system (26) is stable (in the energy norm). As solutions can be obtained on any grid, the grid may be chosen on basis of the required accuracy. But, how accurate is the symmetry-preserving discretization (26)? Before addressing this question (in Section 4.2), we will further enhance the asymptotic order of convergence.

2.3. Higher-order, symmetry-preserving approximation

To turn Eq. (14) into a higher-order approximation, we write down the transport of momentum of a region $\Omega^{(3)}_{i+1/2,j} = [x_{i-3/2}, x_{i+3/2}] \times [y_{j-2}, y_{j+1}]$. Here, it may be noted that we cannot blow up the 'original' volumes $\Omega_{i+1/2,j}$ by a factor of two (in all directions) since our grid is not collocated. On a staggered grid, three times larger volumes are the smallest ones possible for which the same discretization rule can be applied as for the 'original' volumes. This yields

$$|\Omega^{(3)}_{i+1/2,j}| \frac{\mathrm{d}u_{i,j}}{\mathrm{d}t} + \bar{\bar{\boldsymbol{u}}}_{i+3/2,j} u_{i+3/2,j} + \bar{\bar{\boldsymbol{v}}}_{i+1/2,j+1} u_{i,j+3/2} - \bar{\bar{\boldsymbol{u}}}_{i-3/2,j} u_{i-3/2,j} - \bar{\bar{\boldsymbol{v}}}_{i+1/2,j-2} u_{i,j-3/2}, \tag{27}$$

where

$$\bar{\bar{\boldsymbol{u}}}_{i,j} = \int_{y_{j-2}}^{y_{j+1}} u(x_i, y, t)\,\mathrm{d}y \quad \text{and} \quad \bar{\bar{\boldsymbol{v}}}_{i,j} = \int_{x_{i-2}}^{x_{i+1}} v(x, y_j, t)\,\mathrm{d}y. \tag{28}$$

The velocities at the control faces of the large volumes are interpolated to the control faces in a way similar to that given by Eq. (15):

$$u_{i+3/2,j} = \frac{1}{2}(u_{i+3,j} + u_{i,j}) \quad \text{and} \quad u_{i,j+3/2} = \frac{1}{2}(u_{i,j+3} + u_{i,j}). \tag{29}$$

We conceive Eq. (27) as an expression for the velocities, where the mass fluxes $\bar{\bar{\boldsymbol{u}}}$ and $\bar{\bar{\boldsymbol{v}}}$ form the coefficients. Considering it like that, we can recapitulate the equations above (together with the analogous set for the v-component) by

$$\boldsymbol{\Omega}_3 \frac{\mathrm{d}\boldsymbol{u}_h}{\mathrm{d}t} + \boldsymbol{C}_3(\bar{\bar{\boldsymbol{u}}})\boldsymbol{u}_h, \tag{30}$$

where the diagonal matrix $\boldsymbol{\Omega}_3$ represents the sizes of the large control volumes and $\boldsymbol{C}_3$ consists of flux contributions ($\bar{\bar{\boldsymbol{u}}}$ and $\bar{\bar{\boldsymbol{v}}}$) through the faces of these volumes.

On a uniform grid the local truncation errors in Eqs. (18) and (30) are of the order $2 + d$, where $d = 2$ in two spatial dimensions and $d = 3$ in 3D. The leading term in the discretization error may be removed through a Richardson extrapolation (just like in [19]). This leads to the fourth-order approximation

$$\boldsymbol{\Omega} \frac{\mathrm{d}\boldsymbol{u}_h}{\mathrm{d}t} + \left(3^{2+d}\boldsymbol{C}_1(\bar{\boldsymbol{u}}) - \boldsymbol{C}_3(\bar{\bar{\boldsymbol{u}}})\right)\boldsymbol{u}_h,$$

where $\boldsymbol{\Omega} = 3^{2+d}\boldsymbol{\Omega}_1 - \boldsymbol{\Omega}_3$. More specifically, we replace the second-order discretization (16) by the following fourth-order convective discretization

$$\left(3^{2+d}|\Omega_{i+1/2,j}| - |\Omega^{(3)}_{i+1/2,j}|\right)\frac{\mathrm{d}u_{i,j}}{\mathrm{d}t} + 3^{2+d}\frac{1}{2}(\bar{u}_{i+1/2,j} + \bar{v}_{i+1/2,j} - \bar{u}_{i-1/2,j} - \bar{v}_{i+1/2,j-1})u_{i,j}$$
$$+ 3^{2+d}\frac{1}{2}(\bar{u}_{i+1/2,j}u_{i+1,j} - \bar{u}_{i-1/2,j}u_{i-1,j} + \bar{v}_{i+1/2,j}u_{i,j+1} - \bar{v}_{i+1/2,j-1}u_{i,j-1})$$
$$-\frac{1}{2}(\bar{\bar{u}}_{i+3/2,j} + \bar{\bar{v}}_{i+1/2,j+1} - \bar{\bar{u}}_{i-3/2,j} - \bar{\bar{v}}_{i+1/2,j-2})u_{i,j}$$
$$-\frac{1}{2}\left(\bar{\bar{u}}_{i+3/2,j}u_{i+3,j} - \bar{\bar{u}}_{i-3/2,j}u_{i-3,j} + \bar{\bar{v}}_{i+1/2,j+1}u_{i,j+3} - \bar{\bar{v}}_{i+1/2,j-2}u_{i,j-3}\right).$$

To eliminate the leading term of the discretization error in the continuity equation, we apply the law of conservation of mass to $\Omega^{(3)}_{i,j} = [x_{i-2}, x_{i+1}] \times [y_{j-2}, y_{j+1}]$:

$$\bar{\bar{u}}_{i+1,j} + \bar{\bar{v}}_{i,j+1} - \bar{\bar{u}}_{i-2,j} - \bar{\bar{v}}_{i,j-2} = 0, \tag{31}$$

where the fluxes $\bar{\bar{u}}_{i,j}$ and $\bar{\bar{v}}_{i,j}$ are approximated in terms of the discrete velocities $u_{i,j}$ and $v_{i,j}$, respectively,

$$\bar{\bar{u}}_{i,j} = (y_{j+1} - y_{j-2})u_{i,j} \quad \text{and} \quad \bar{\bar{v}}_{i,j} = (x_{i+1} - x_{i-2})v_{i,j}. \tag{32}$$

That is on a uniform grid, the fluxes $\bar{\bar{u}}_{i,j}$ and $\bar{\bar{v}}_{i,j}$ are approximated by means of the mid-point rule. The fourth-order approximation of the law of conservation of mass becomes

$$3^{2+d}(\bar{u}_{i,j} + \bar{v}_{i,j} - \bar{u}_{i-1,j} - \bar{v}_{i,j-1}) - (\bar{\bar{u}}_{i+1,j} + \bar{\bar{v}}_{i,j+1} - \bar{\bar{u}}_{i-2,j} - \bar{\bar{v}}_{i,j-2}) = 0, \tag{33}$$

or in matrix-vector notation

$$\boldsymbol{M}\boldsymbol{u}_h = (3^{2+d}\boldsymbol{M}_1 - \boldsymbol{M}_3)\boldsymbol{u}_h = \boldsymbol{0}, \tag{34}$$

where we have summarized the discretization of the law of conservation of mass applied to the volumes $\Omega^{(3)}_{i,j}$ by $\boldsymbol{M}_3\boldsymbol{u}_h = \boldsymbol{0}$. The weights 3^{2+d} and -1 are to be used on non-uniform grids too, since otherwise the symmetry of the underlying differential operator is lost.

As noted before, the matrix $\boldsymbol{C}_1 - \mathrm{diag}(\boldsymbol{C}_1)$ is skew-symmetric, because the velocities at the control faces are interpolated with constant coefficients. The same holds for $\boldsymbol{C}_3$. The matrix $\boldsymbol{C}_3 - \mathrm{diag}(\boldsymbol{C}_3)$ is skew-symmetric for all interpolations of $\bar{\bar{\boldsymbol{u}}}$ and $\bar{\bar{\boldsymbol{v}}}$ to the control faces, since the velocities at the control faces are interpolated with constant coefficients, see (29). Hence, without diagonal the coefficient matrix $3^{2+d}\boldsymbol{C}_1(\bar{\boldsymbol{u}}) - \boldsymbol{C}_3(\bar{\bar{\boldsymbol{u}}})$ is skew-symmetric.

For skew-symmetry the interpolation of the $\bar{u}$'s, $\bar{v}$'s, $\bar{\bar{u}}$'s and $\bar{\bar{v}}$'s to the control faces has to be performed in such a way that the diagonal entries

$$3^{2+d}\frac{1}{2}(\bar{u}_{i+1/2,j} + \bar{v}_{i+1/2,j} - \bar{u}_{i-1/2,j} - \bar{v}_{i+1/2,j-1}) - \frac{1}{2}(\bar{\bar{u}}_{i+3/2,j} + \bar{\bar{v}}_{i+1/2,j+1} - \bar{\bar{u}}_{i-3/2,j} - \bar{\bar{v}}_{i+1/2,j-2}) \tag{35}$$

of the convective matrix $3^{2+d}\boldsymbol{C}_1(\bar{\boldsymbol{u}}) - \boldsymbol{C}_3(\bar{\bar{\boldsymbol{u}}})$ become equal to zero, that is equal to linear combinations of (33). To achieve this, we interpolate $\bar{u}_{i+1/2,j}$ in the following manner

$$\bar{u}_{i+1/2,j} = \frac{1}{2}\alpha(\bar{u}_{i+1,j} + \bar{u}_{i,j}) + \frac{1}{2}(1-\alpha)(\bar{u}_{i+2,j} + \bar{u}_{i-1,j}), \tag{36}$$

where α is a constant, and interpolate $\bar{v}_{i+1/2,j}$, $\bar{\bar{u}}_{i+1/2,j}$ and $\bar{\bar{v}}_{i+1/2,j}$ likewise. As in Morinishi et al. [4] we take $\alpha = 9/8$ because all interpolations are fourth-order accurate then (on a uniform grid). Note that the

convective discretization is conservative for any value of α, and fourth-order accurate if $\alpha = 9/8$. We cannot take $\alpha = 1$ (as in the second-order method, see Eq. (21)) since the Richardson extrapolation does not eliminate the second-order terms in the error in the interpolations of $\bar{\bar{u}}_{i+1/2,j}$ and $\bar{\bar{v}}_{i+1/2,j}$. The interpolation rule (36) is also applied in the j-direction to approximate the flux through the faces of v-cells. After that the interpolation rule (36) is applied, and the flux is expressed in terms of the discrete velocity like in (22) and (32), the coefficient matrix $3^{2+d}\boldsymbol{C}_1(\bar{\boldsymbol{u}}) - \boldsymbol{C}_3(\bar{\bar{\boldsymbol{u}}})$ becomes a function of the discrete velocity vector $\boldsymbol{u}_h$ only. We denote that function by $\boldsymbol{C}(\boldsymbol{u}_h)$.

The leading error of the diffusive discretization may be eliminated in two different ways. We may either resort to

$$\frac{1}{Re}\left(3^{2+d}\boldsymbol{\Delta}_1^*\boldsymbol{\Lambda}_1^{-1}\boldsymbol{\Delta}_1 - \boldsymbol{\Delta}_3^*\boldsymbol{\Lambda}_3^{-1}\boldsymbol{\Delta}_3\right),$$

or take the fourth-order coefficient matrix like

$$\boldsymbol{D} = \frac{1}{Re}\left(3^{2+d}\boldsymbol{\Delta}_1 - \boldsymbol{\Delta}_3\right)^*\left(3^{2+d}\boldsymbol{\Lambda}_1 - \boldsymbol{\Lambda}_3\right)^{-1}\left(3^{2+d}\boldsymbol{\Delta}_1 - \boldsymbol{\Delta}_3\right), \tag{37}$$

where the difference matrix $\boldsymbol{\Delta}_3$ and the diagonal matrix $\boldsymbol{\Lambda}_3$ are the relatives of $\boldsymbol{\Delta}_1$ and $\boldsymbol{\Lambda}_1$, respectively, with the difference that they are defined on 3^d-times larger control volumes. The larger number of nonzero entries may be counted against (37). Yet this drawback is more than counterbalanced when the structure of the discrete approximation is considered. Like the underlying differential operator $\nabla^*\nabla = -\nabla\cdot\nabla$, the right-hand side of (37) consists of a gradient matrix, $3^{2+d}\boldsymbol{\Delta}_1 - \boldsymbol{\Delta}_3$, and its transpose. For that reason we opt for the diffusive matrix given by (37). In terms of the abbreviations $\boldsymbol{\Delta} = 3^{2+d}\boldsymbol{\Delta}_1 - \boldsymbol{\Delta}_3$ and $\boldsymbol{\Lambda} = 3^{2+d}\boldsymbol{\Lambda}_1 - \boldsymbol{\Lambda}_3$ we have $\boldsymbol{D} = \boldsymbol{\Delta}^*\boldsymbol{\Lambda}^{-1}\boldsymbol{\Delta}/Re$. The quadratic form

$$\boldsymbol{u}_h^*\boldsymbol{D}\boldsymbol{u}_h = \frac{1}{Re}(\boldsymbol{\Delta}\boldsymbol{u}_h)^*\boldsymbol{\Lambda}^{-1}(\boldsymbol{\Delta}\boldsymbol{u}_h)$$

is non-negative provided that the entries of the diagonal matrix $\boldsymbol{\Lambda}$ are non-negative. Here, we assume that the grid is chosen such that this condition is satisfied. Note that $\boldsymbol{\Lambda}_{ii} < 0$ for some i implies that the grid is so irregular that is does not make sense to apply a fourth-order method; in that case the second-order method (26) should be applied. For $\boldsymbol{\Lambda} > \boldsymbol{0}$, the quadratic form $\boldsymbol{u}_h^*\boldsymbol{D}\boldsymbol{u}_h$ equals zero if and only if $\boldsymbol{\Delta}\boldsymbol{u}_h = \boldsymbol{0}$, that is if and only if the discrete gradient of the velocity equals zero. This is precisely the condition that need be satisfied in the continuous case. Indeed, in the continuous case we have

$$-\int \boldsymbol{u}\nabla\cdot\nabla\boldsymbol{u}\,\mathrm{d}V = \int |\nabla\boldsymbol{u}|^2\,\mathrm{d}V = 0,$$

if and only if $\nabla\boldsymbol{u} = \boldsymbol{0}$.

Now, taking all ingredients together, the symmetry-preserving discretization of the Navier–Stokes equations (1) becomes

$$\boldsymbol{\Omega}\frac{\mathrm{d}\boldsymbol{u}_h}{\mathrm{d}t} + \boldsymbol{C}(\boldsymbol{u}_h)\boldsymbol{u}_h + \boldsymbol{D}\boldsymbol{u}_h - \boldsymbol{M}^*\boldsymbol{p}_h = \boldsymbol{0}, \quad \boldsymbol{M}\boldsymbol{u}_h = \boldsymbol{0}, \tag{38}$$

where the convective coefficient matrix $\boldsymbol{C}(\boldsymbol{u}_h)$ is skew-symmetric, like a first-order differential operator, the discrete diffusive operator $\boldsymbol{D}$ is symmetric and positive-definite, and all terms are consistently discretized, that is $\boldsymbol{C}(\boldsymbol{u}_h)\boldsymbol{1} = \boldsymbol{0}$, $\boldsymbol{D}\boldsymbol{1} = \boldsymbol{0}$ and $\boldsymbol{M}\boldsymbol{1} = \boldsymbol{0}$. Repeating the analysis of Section (2.2), for the fourth-order discretization, shows that the symmetry-preserving discretization (38) is stable and conserves mass, momentum and energy.

2.4. Boundary conditions

So far, we have left the boundary conditions out of consideration. Obviously, their numerical treatment has to maintain the symmetry properties. In case of periodic conditions, the discretization can be extended up to the boundaries in a natural way. This does not break the symmetries of the coefficient matrices $\boldsymbol{C}$ and $\boldsymbol{D}$ nor does it conflict with consistency conditions. Thus for periodic boundary conditions both stability and conservation properties are maintained.

Also for non-periodic boundary conditions, the convective and diffusive differential operators can be discretized in such a way that their symmetry properties are preserved. Below we will describe a symmetry-preserving discretization near/at a no-slip boundary. Other types of boundary conditions can be handled in the same vein.

To start, we consider the discretization of mass fluxes near a no-slip boundary. The situation is sketched in Fig. 4 (left). In this figure, the wall is given by the grid line $j = 0$, and the fluid occupies the region $j > 0$.

Since the wall is impervious, we have

$$\bar{v}_{i,0} = \bar{\bar{v}}_{i,0} = 0. \tag{39}$$

Note that a single overbar denotes the integration over one grid face, see Eq. (13), whereas a double overbar stands for the integration over three grid faces, see Eq. (28). To apply the discrete law of conservation of mass up to the wall, we extent the grid by mirroring it in the wall $j = 0$. Then, for $j = 1$ the discretization of the law of conservation of mass (Eq. (33)) becomes

$$3^{2+d}(\bar{u}_{i,1} + \bar{v}_{i,1} - \bar{u}_{i-1,1} - \bar{v}_{i,0}) - (\bar{\bar{u}}_{i+1,1} + \bar{\bar{v}}_{i,2} - \bar{\bar{u}}_{i-2,1} - \bar{\bar{v}}_{i,-1}) = 0,$$

where the mass flux $\bar{\bar{v}}_{i,-1}$ is located outside of the flow domain. To define the out-of-domain flux $\bar{\bar{v}}_{i,-1}$ we impose that the net mass flow through the wall-centered control volume $[x_{i-2}, x_{i+1}] \times [y_{-1}, y_1]$ (depicted in Fig. 4, right) equals zero, where we assume that the mass flux through faces normal to the wall vanishes ($\bar{u}_{i,1} + \bar{u}_{i,0} = 0$, for any i) because the no-slip condition states that the u-velocity is zero at the mid of these faces. We therefore define the out-of-domain flux by

$$\bar{\bar{v}}_{i,-1} = \bar{\bar{v}}_{i,1}. \tag{40}$$

Note that this relation defines the boundary treatment for both the continuity constraint $\boldsymbol{M}\boldsymbol{u}_h = \boldsymbol{0}$ and the discrete pressure term $\boldsymbol{M}^*\boldsymbol{p}_h$.

The discretization of the convective flux near the boundary has to be done such that the skew-symmetry of $\boldsymbol{C}$ is preserved. Here, we have to distinguish between the wall-normal and tangential velocity, since the

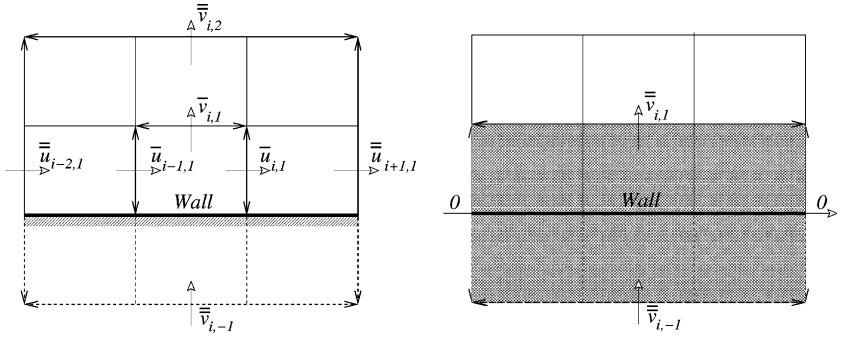

Fig. 4. The left-hand figure depicts the mass fluxes that are used to discretize the law of conservation of mass near the no-slip wall $j = 0$. The right-hand figure shows the control volume that is applied to define the out-of-domain mass flux $\bar{\bar{v}}_{i,-1}$.

velocities are staggered. The tangential velocity $u_{i,j}$ is computed from 3^{d+2} Eqs. (14)–(27) for $j = 1, 2, 3, \ldots$ Therefore the last term in Eq. (27), that is the convective flux $\bar{\bar{v}}_{i+1/2,j-2}u_{i,j-3/2}$, need be defined for $j = 1$ and $j = 3$. Note that for $j = 2$ this flux is evaluated at the wall, and thus given by Eq. (39). The same holds for the term $\bar{v}_{i+1/2,0}u_{i,1/2}$ in Eq. (14). Interpolating the velocity as in (29) gives

$$\bar{\bar{v}}_{i+1/2,j-2}u_{i,j-3/2} = \bar{\bar{v}}_{i+1/2,j-2}\frac{1}{2}(u_{i,j} + u_{i,j-3}).$$

The out-of-domain velocity $u_{i,0}$ (which appears in the expression above for $j = 3$) is defined by means of the no-slip condition $u_{i,0} + u_{i,1} = 0$. The out-of-domain mass flux $\bar{\bar{v}}_{i+1/2,-1}$ is computed according to Eq. (40). This leads to

$$\bar{\bar{v}}_{i+1/2,j-2}u_{i,j-3/2} = \begin{cases} \bar{\bar{v}}_{i+1/2,1}\frac{1}{2}(u_{i,3} - u_{i,1}) & \text{for } j = 3; \\ \bar{\bar{v}}_{i+1/2,1}\frac{1}{2}(u_{i,1} + u_{i,-2}) & \text{for } j = 1. \end{cases}$$

Hence, the discretization is skew-symmetric if and only if $u_{i,-2} = u_{i,3}$.

To compute the normal velocity $v_{i,j}$ near the wall $j = 0$, we extend the discrete law of conservation of mass (Eq. (33)) to $j = 0$ by taking

$$\bar{\bar{u}}_{i,0} + \bar{\bar{u}}_{i,1} = 0, \bar{v}_{i,-1} - \bar{v}_{i,1} = 0 \quad \text{and} \quad \bar{\bar{v}}_{i,-2} - \bar{\bar{v}}_{i,2} = 0. \tag{41}$$

Now, Eq. (33) holds also for $j = 0$ (provided that it holds for $j = 1$) and we need only define the convective flux

$$\bar{\bar{v}}_{i,j-3/2}v_{i,j-3/2} = \frac{1}{2}\left(\bar{\bar{v}}_{i,j} + \bar{\bar{v}}_{i,j-3}\right)\frac{1}{2}(v_{i,j} + v_{i,j-3}) \quad \text{for } j = 1, 2,$$

where the out-of-domain mass fluxes $\bar{\bar{v}}_{i,-1}$ and $\bar{\bar{v}}_{i,-2}$ are given by Eq. (40) and (41), respectively. The out-of-domain velocity $v_{i,-1}$ is determined with the help of the no-slip condition, $v_{i,-1} + v_{i,1} = 0$, and $v_{i,-2}$ follows from the requirement that the discretization is skew-symmetric. By writing down the discretization

$$\bar{\bar{v}}_{i,j-3/2}v_{i,j-3/2} = \begin{cases} \frac{1}{2}(\bar{\bar{v}}_{i,2} + \bar{\bar{v}}_{i,1})\frac{1}{2}(v_{i,2} - v_{i,1}) & \text{for } j = 2; \\ \frac{1}{2}(\bar{\bar{v}}_{i,1} + \bar{\bar{v}}_{i,2})\frac{1}{2}(v_{i,1} + v_{i,-2}) & \text{for } j = 1, \end{cases}$$

we see that $v_{i,-2}$ has to be taken equal to $v_{i,2}$.

In summary, like the convective discretization away from the boundary, the discretization near the boundary is not constructed to minimize the local truncation error. Instead, we have built the no-slip condition into the coefficient matrix $\boldsymbol{C}$ without violating the skew-symmetry. Consequently, also for no-slip conditions, the kinetic energy is conserved if $\boldsymbol{D} = \boldsymbol{0}$.

The diffusive fluxes through near-wall control faces ought to be discretized such that the resulting coefficient matrix $\boldsymbol{D}$ is symmetric and positive-definite. Eq. (37) writes $\boldsymbol{D}$ as $\boldsymbol{\Delta}^*\boldsymbol{\Lambda}\boldsymbol{\Delta}$, where $\boldsymbol{\Lambda}$ is a positive diagonal matrix. Consequently, the matrix $\boldsymbol{D}$ remains symmetric and positive-definite when the discrete no-slip conditions $u_{i,0} + u_{i,1} = 0$, $u_{i,-1} + u_{i,2} = 0$, $u_{i,-2} + u_{i,3} = 0$, $v_{i,-1} + v_{i,1} = 0$ and $v_{i,-2} + v_{i,2} = 0$ are built into the difference matrix $\boldsymbol{\Delta} = 3^{2+d}\boldsymbol{\Delta}_1 - \boldsymbol{\Delta}_3$ and Eq. (37) is applied to construct $\boldsymbol{D}$.

3. Time-integration method

The time-derivative in Eq. (38) has to be replaced by a skew-symmetric discrete operator to preserve the favorable conservation and stability properties for discrete time too. This can only be achieved when the time-integration is done implicitly. Introducing the time step δt and denoting the velocity and pressure at

time $t = n\delta t$ by $\boldsymbol{u}_h^n$ and $\boldsymbol{p}_h^n$, respectively, we may integrate Eq. (38) over one step in time by means of the midpoint rule, for example, which leads to

$$\boldsymbol{\Omega}\frac{\boldsymbol{u}_h^{n+1}-\boldsymbol{u}_h^n}{\delta t}+\boldsymbol{C}\left(\boldsymbol{u}_h^{n+1/2}\right)\boldsymbol{u}_h^{n+1/2}+\boldsymbol{D}\boldsymbol{u}_h^{n+1/2}-\boldsymbol{M}^*\boldsymbol{p}_h^{n+1/2}=\boldsymbol{0},\quad \boldsymbol{M}\boldsymbol{u}_h^{n+1}=\boldsymbol{0},$$

where the mid-step velocity is given by $\boldsymbol{u}_h^{n+1/2}=\frac{1}{2}(\boldsymbol{u}_h^{n+1}+\boldsymbol{u}_h^n)$. This second-order, skew-symmetric approximation conserves the energy in the absence of diffusion, and is unconditionally stable in the presence of diffusion. Indeed, taking the inner product with the mid-step velocity gives

$$\boldsymbol{u}_h^{n+1^*}\boldsymbol{\Omega}\boldsymbol{u}_h^{n+1}-\boldsymbol{u}_h^{n*}\boldsymbol{\Omega}\boldsymbol{u}_h^n=-\delta t\boldsymbol{u}_h^{n+1/2*}(\boldsymbol{D}+\boldsymbol{D}^*)\boldsymbol{u}_h^{n+1/2}\leqslant 0.$$

Note that this (in)equality also holds when the convective coefficient matrix is evaluated at the old time level n, i.e., becomes $\boldsymbol{C}(\boldsymbol{u}_h^n)$. The associated linear method is the simplest—read: cheapest possible—implicit method. Yet, for the use in direct numerical simulations of turbulent flow the computational costs are rather high compared to those of explicit methods. In view of the lower costs, we consider explicit methods in the remainder of this section.

For inviscid flows, we can partially escape from the necessity for treating convection implicit by adopting the leapfrog method

$$\boldsymbol{\Omega}\frac{\boldsymbol{u}_h^{n+1/2}-\boldsymbol{u}_h^{n-1/2}}{\delta t}+\boldsymbol{C}\left(\boldsymbol{u}_h^n\right)\boldsymbol{u}_h^n-\boldsymbol{M}^*\boldsymbol{p}_h^n=\boldsymbol{0},\quad \boldsymbol{M}\boldsymbol{u}_h^{n+1}=\boldsymbol{0},$$

where the pressure $\boldsymbol{p}_h^n$ is to be computed such that the incompressibility constraint is satisfied at time $t=(n+1)\delta t$. Now, taking the inner product with $\boldsymbol{u}_h^n$ shows that the quantity $\boldsymbol{u}_h^{n+1*}\boldsymbol{\Omega}\boldsymbol{u}_h^n$ is conserved in time. So, if we loosely view this (not necessarily positive) quantity as the 'energy', we have conservation built into the discrete system. Yet, this statement is not as strong as the results obtained before, because $\boldsymbol{u}_h^{n+1*}\boldsymbol{\Omega}\boldsymbol{u}_h^n$ is not a norm. As we do not have a proper energy norm, we do not get unconditional stability from conservation of energy: the leapfrog method is stable if and only if the time step is smaller than the largest (measured in absolute value) eigenvalue of $\boldsymbol{C}$.

The leapfrog method becomes unstable when diffusion is added. Therefore it need be modified to handle viscous flow. We consider modifications of the form

$$\boldsymbol{\Omega}\frac{\boldsymbol{u}_h^{n+\beta+1/2}-\boldsymbol{u}_h^{n+\beta-1/2}}{\delta t}+\boldsymbol{C}\left(\boldsymbol{u}_h^{n+\beta}\right)\boldsymbol{u}_h^{n+\beta}+\boldsymbol{D}\boldsymbol{u}_h^{n+\beta}-\boldsymbol{M}^*\boldsymbol{p}_h^{n+\beta}=\boldsymbol{0}. \tag{42}$$

where the off-step velocities are given by

$$\boldsymbol{u}_h^{n+\beta+1/2}=\left(\beta+\frac{1}{2}\right)\boldsymbol{u}_h^{n+1}-\left(\beta-\frac{1}{2}\right)\boldsymbol{u}_h^n\quad\text{and}\quad \boldsymbol{u}_h^{n+\beta}=(1+\beta)\boldsymbol{u}_h^n-\beta\boldsymbol{u}^{n-1}.$$

The incompressibility constraint is treated implicit (as before). Substituting the linear inter-/extrapolations for the off-step velocities into Eq. (42) yields a family of one-leg methods (so-called because it uses just one evaluation of the flux per time-step) parameterized by β. Our aim is now to determine β such that the corresponding method possesses the largest region of stability. Since both the pressure and the incompressibility constraint are treated implicit in time, we may discard them when stability is considered. Therefore we focus on the one-leg scheme for the simplified, one-dimensional test problem $\partial_t u=f(u)$. For this problem the one-leg scheme reads

$$\left(\beta+\frac{1}{2}\right)u^{n+1}-2\beta u^n+\left(\beta-\frac{1}{2}\right)u^{n-1}=\delta t f((1+\beta)u^n-\beta u^{n-1}). \tag{43}$$

The temporal discretization (43) is second-order accurate for all $\beta \neq -1/3$, and third-order accurate when $\beta = -1/3$. The error constant is given by $C_3 = (1 + 3\beta)/6$.

Taking $\beta = 1/2$, we have a one-leg method which is the twin of Adams–Bashforth. According to Adams–Bashforth we ought to take $\frac{3}{2}f(u^n) - \frac{1}{2}f(u^{n-1})$ instead of $f(\frac{3}{2}u^n - \frac{1}{2}u^{n-1})$. These methods are identical if f is linear, and thus have the same region of linear stability. Differences occur for nonlinear right-hand sides f.

We look for the one-leg method with the best linear stability properties, where we consider the popular method of Adams and Bashforth as point of reference. Fig. 5 (left) shows the stability domain of the one-leg method for $\beta = 0.05$ and $\beta = 0.5$ (Adams–Bashforth). The stability domain is pressed against the imaginary axis when β goes to zero. In the limit $\beta = 0$ the stability domain is equal to the interval $[-i, i]$, i.e., to leapfrog's stability region.

The time step δt of an explicit time integration method for a convection–diffusion equation is typically restricted by a convective stability condition like $U\delta t < \delta y$ (where U denotes the absolute maximum of the velocity and δy stands for the spatial mesh size), and a diffusive stability condition of the form $2\delta t < Re\delta y^2$. For the numerical simulation of the flow in the channel at $Re = 5600$ we use mesh sizes of the order 5×10^{-3}. The maximal velocity U equals one. Hence, the convective stability condition is about fourteen times stronger than the diffusive condition. Therefore, we look for stability domains which include eigenvalues $\lambda = x + \mathrm{i}y$, where the real part x is negative and the absolute value of the imaginary part y is much larger than the absolute value of the real part. Under these conditions, the one-leg method with $\beta = 0.05$ outperforms Adams–Bashforth. Fig. 5 (right) shows a blow up of the stability domains of both methods near the positive imaginary axis. The points denoted by A and B lie on the line $|x| : |y| = 1 : 20$. The point A lies close to the boundary of the stability domain for $\beta = 0.05$; B lies near to the boundary of the stability domain for $\beta = 0.5$. A lies approximately two times as far from the origin as B. Thus, the time step of the one-leg method with $\beta = 0.05$ can be enlarged by a factor of two compared to Adams–Bashforth. For $|x| : |y| = 1 : 10$ this factor is about 1.5; for $|x| : |y| = 1 : 100$ it is approximately 2.5.

We have carried out a number of numerical test calculations which showed that the one-leg method with $\beta = 0.05$ requires indeed about two times less computational effort than the second-order method of Adams and Bashforth, whereas the accuracy is as good or better. In practice, we choose the time-step such that the time-integration becomes unstable when the selected time-step is enlarged by 25%.

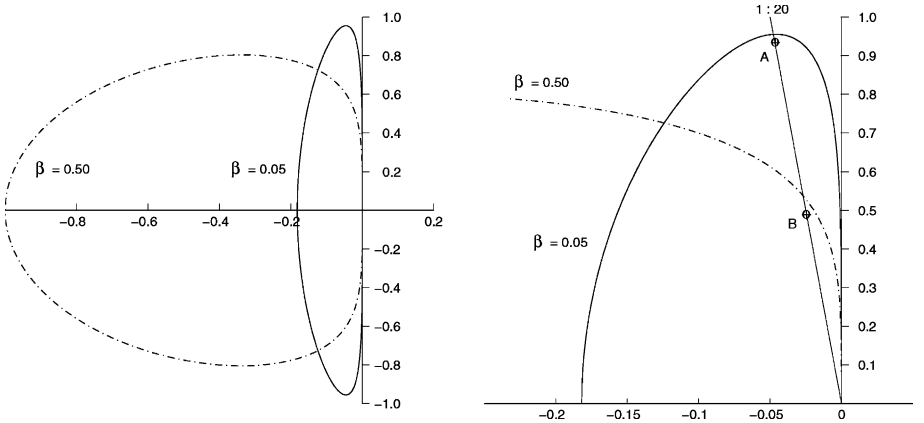

Fig. 5. The left picture shows the stability domain of the one-leg method (43) for $\beta = 0.05$ and $\beta = 0.5$. The right picture shows a blow up of the stability domains near the positive imaginary axis.

4. How accurate is the symmetry-preserving discretization?

We will demonstrate the performance of the above second and fourth-order symmetry-preserving discretization methods with the help of two test-cases. The first test-case is the one-dimensional convection–diffusion equation (5) for which the steady, analytical solution is known (Section 4.1). The second case deals with a fully developed channel flow. The unsteady Navier–Stokes equations are solved numerically at a Reynolds number of $Re = 5600$, which is based on the mean bulk velocity and the channel height (based on the channel half-width and wall shear velocity the Reynolds number reads 180). At this Reynolds number the channel flow has been studied intensively. A large number of numerical results as well as experimental data is available for comparison (see Section 4.2).

4.1. Comparison with traditional discretization methods

To kick off, the symmetry-preserving discretization is compared with the traditional discretization methods based on Lagrange interpolation (minimizing local truncation error) for the steady version of the one-dimensional convection–diffusion equation (5). Since on uniform grids the methods are equal, we choose an example with a boundary-layer character, requiring grid refinement near the outflow boundary $x = 1$. This is achieved by imposing the boundary conditions $u(0,t) = 0$ and $u(1,t) = 1$. The parameters in Eq. (5) are set equal to $\bar{u} = 1$ and $Re = 1000$.

Grid refinement has been carried out on an exponentially stretched grid, with half the grid points in the thin boundary layer of thickness $10/Re$ near $x = 1$. Four discretization methods have been investigated: the traditional Lagrangian second-order method (2L) and its fourth-order counterpart (denoted by 4L), and the second-order (2S) and fourth-order (4S) symmetry-preserving methods. For 4L we have implemented exact boundary conditions to circumvent the problem of a difference molecule that is too large near the boundary.

We form the vector $\boldsymbol{u}_{\text{exact}}$ by restricting the analytical solution of Eq. (5) to the grid points, and monitor the global discretization error defined by $\|\boldsymbol{u}_h - \boldsymbol{u}_{\text{exact}}\|$ (where the norm is the kinetic energy norm). Fig. 6 shows the global error as a function of the mean mesh size $1/N$, where N is the number of grid points.

A number of observations can be made.

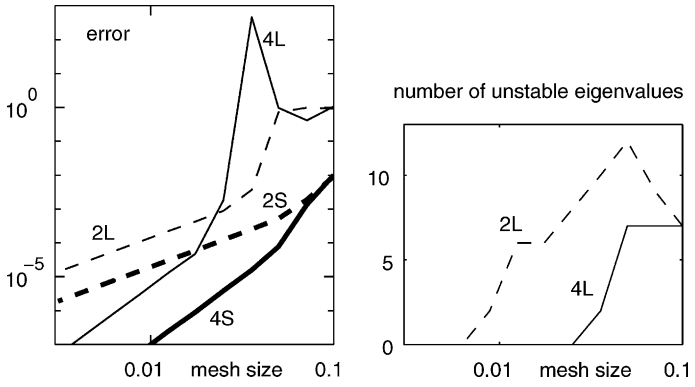

Fig. 6. The left-hand figure shows the global error as a function of the mean mesh size on an exponential grid with half of the grid points inside a boundary layer of thickness $10/Re$. Four methods are shown: 2L and 4L (second- and fourth-order Lagrangian), 2S and 4S (second- and fourth-order symmetry-preserving). The right-hand figure depicts the number of eigenvalues of the Lagrangian methods 2L and 4L located in the unstable half-plane. Only the Lagrangian methods are shown, since the symmetry-preserving discretization keeps all the eigenvalues in the stable half-plane.

- For all grid sizes the Lagrangian discretization appears to be less accurate than the symmetry-preserving alternative.
- For coarser grids the fourth-order Lagrangian method is not even as accurate as its second-order Lagrangian relative. Similar observations have been made frequently, and this explains why thus far fourth-order discretization has not been very popular.
- The symmetry-preserving methods already behave nicely on coarse grids. Moreover they show a regular monotone behavior upon grid refinement. As in turbulent-flow simulations one will always have to cope with limitations on the affordable number of grid points, methods that are less sensitive in this respect are preferable.
- Also note that for a given accuracy (say 10^{-5}), the grid size of the fourth-order symmetry-preserving method can be chosen roughly three times larger than that of the fourth-order Lagrangian method!
- The fourth-order Lagrangian method nearly breaks down for $N = 28$ where the stretching factor is 0.72 (which is not extreme). This is due to an eigenvalue moving from the unstable half-plane (for low values of N), towards the stable half-plane (for higher N), which crosses the imaginary axis close to the origin, making the coefficient matrix almost singular. When one or more eigenvalues of the coefficient matrix are located in the unstable half-plane, the corresponding time-dependent, semi-discrete system is unstable, and can not be integrated in the time domain. In the above examples we have computed the discrete steady-state by a direct matrix solver to avoid this problem.

4.2. A more challenging test-case: fully developed channel flow

The symmetry-preserving discretization is tested for turbulent channel flow. The Reynolds number is set equal to $Re = 5600$ (based on the channel width and the bulk velocity), a Reynolds number at which direct numerical simulations have been performed by several research groups; see [20–22]. Additionally, we can compare the numerical results to experimental data from Kreplin and Eckelmann [23]. They have measured the flow in the wall region of a channel at a somewhat higher Reynolds number of approximately 6,600 (based on the channel width and the bulk velocity). Yet, this difference is insignificant: Eckelmann [24] reports in an earlier paper that the root-mean-squares of fluctuating velocities at $Re = 5600$ and $Re = 6600$ collapse onto one curve (provided they are properly normalized by the friction velocity, of coarse).

As usual, the flow is assumed to be periodic in the stream- and spanwise direction. Consequently, the computational domain may be confined to a channel unit of dimension $2\pi \times 1 \times \pi$, where the width of the channel is normalized. All computations presented in this section have been performed with 64 (uniformly distributed) streamwise grid points and 32 (uniformly distributed) spanwise points. In the lower-half of the channel, the wall-normal grid points are computed according to

$$y_j = \frac{\sinh(\gamma j/N_y)}{2\sinh(\gamma/2)} \quad \text{with } j = 0, 1, \ldots, N_y/2,$$

where N_y denotes the number of grid points in the wall-normal direction. The stretching parameter γ is taken equal to 6.5. The grid points in the upper-half are computed by means of symmetry.

The temporal integration is performed with the help of the one-leg method that is outlined in Section 3. The non-dimensional time step is set equal to $\delta t = 1.25 \times 10^{-3}$. Mean values of computational results are obtained by averaging the results over the directions of periodicity, the two symmetrical halves of the channel, and over time. The averaging over time starts after a start-up period. The start-up period as well as the time-span over which the results are averaged, 1500 time-units (non-dimensionalized by the bulk velocity and the channel width), are identical for all the results shown is this section.

Fig. 7 shows a comparison of the mean velocity profile as obtained from our fourth-order symmetry-preserving simulation ($N_y = 64$) with those of direct numerical simulations. The results that we compare

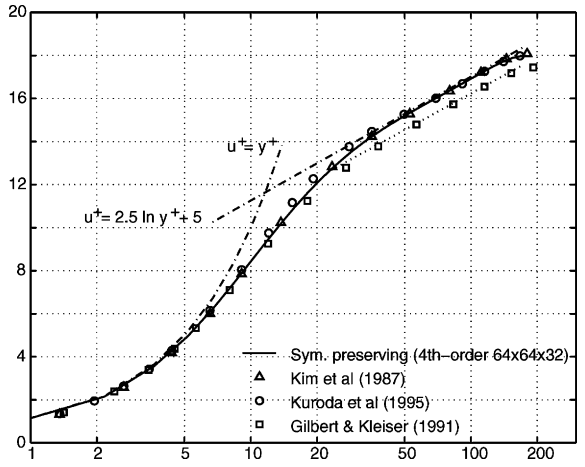

Fig. 7. Comparison of the mean streamwise velocity u^+ as function of y^+. The dashed lines represent the law of the wall and the log law. The markers represent DNS-results that are taken from both the ERCOFTAC Database and the Japanese DNS Data Base of Turbulent Transport Phenomena.

with have all been obtained by means of spectral methods based on truncated Fourier series in the streamwise and spanwise direction, and a Chebyshev polynomial expansion in the normal direction. The computational boxes are precisely, or almost, the same. Yet, the grids used by the spectral methods have 12 times [22], 25 times [21], and 30 times [20] more points than our grid has. In addition, the number of collocation points in the spectral methods is expanded by a factor of 3/2 before transforming the nonlinear terms into the physical space to reduce the aliasing error. Nevertheless, the agreement between our, relatively coarse-grid, results and those of the spectral methods is excellent.

To investigate the convergence of the fourth-order method upon grid refinement, we have monitored the skin friction coefficient C_f as obtained from simulations on five different grids. We will denote these grids by A, B, C, D and E. Their spacings differ only in the direction normal to the wall. They have $N_y = 128$ (grid A), $N_y = 96$ (B), $N_y = 64$ (C), $N_y = 56$ (D) and $N_y = 48$ (E) points in the wall-normal direction, respectively. The first (counted from the wall) grid line used for the convergence study is located at $y_1^+ \approx 0.72$ (grid A), $y_1^+ \approx 0.95$ (B), $y_1^+ \approx 1.4$ (C), $y_1^+ \approx 1.6$ (D), and $y_1^+ \approx 1.9$ (E), respectively. Fig. 8 displays the skin friction

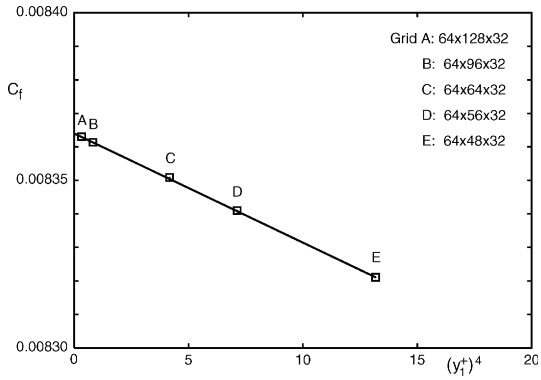

Fig. 8. Convergence of the skin friction coefficient C_f upon grid refinement. The figure displays C_f versus the fourth power of the first grid point y_1^+.

coefficient C_f as function of the fourth power of the local grid spacing (measured by y_1^+). The convergence study shows that the discretization scheme is indeed fourth-order accurate, on a nonuniform mesh. This indicates that the underlying physics is resolved when 48 or more grid points are used in the wall normal direction. The straight line in Fig. 8 is approximately given by $C_f = 0.00836 - 0.000004(y_1^+)^4$. The extrapolated value at the crossing with the vertical axis $y_1^+ = 0$ lies in between the C_f reported by Kim et al. [20] (0.00818) and Dean's correlation of $C_f = 0.073Re^{-1/4} = 0.00844$ [25]. Note that the extrapolation eliminates the (leading term of the) discretization error in the wall-normal direction, but not the other discretization errors in space and time.

The convergence of the fluctuating streamwise velocity near the wall ($0 < y^+ < 20$) is presented in Fig. 9. Here, we have added results obtained on three still coarser grids (with $N_y = 32$, $N_y = 24$ and $N_y = 16$ points in the wall-normal direction, respectively), since the results on the grids A–E fall almost on top of each other. The coarsest grid, with only $N_y = 16$ points to cover the channel width, is coarser than most of the grids used to perform a large-eddy simulation (LES) of this turbulent flow. Nevertheless, the $64 \times 16 \times 32$ solution is not that far off the solution on finer grids, in the near wall region. Further away from the wall, the turbulent fluctuations predicted on the coarse grids ($N_y \leqslant 32$) become too high compared to the fine grid solutions, as is shown in Fig. 10.

Perhaps, the solution on the $64 \times 24 \times 32$ forms an excellent starting point for a large-eddy simulation. The root-mean-square of the fluctuating streamwise velocity is not far of the fine grid solution. Viewed

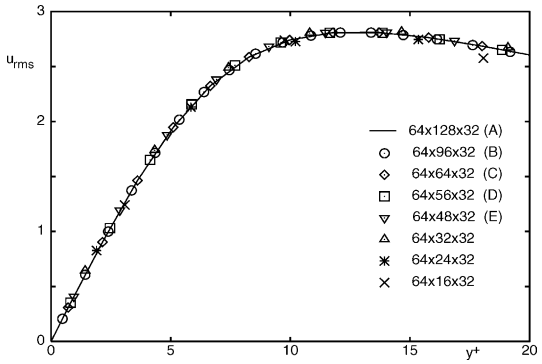

Fig. 9. The root-mean-square velocity fluctuations normalized by the wall shear velocity as function of the wall coordinate y^+ on various grids for $y^+ \leqslant 20$. The markers correspond to the results obtained in the grid points. The solution on the finest grid is represented by a continuous line.

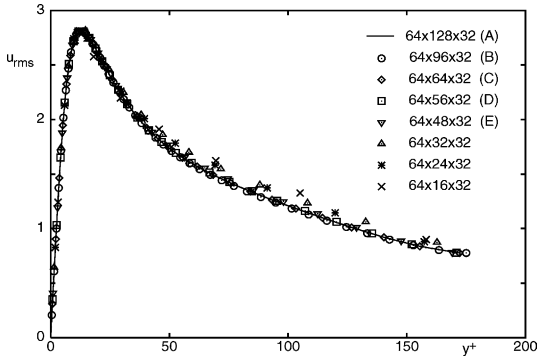

Fig. 10. The root-mean-square velocity fluctuations normalized by the wall shear velocity for $y^+ \leqslant 200$ on various grids.

through physical glasses, the energy of the resolved scales of motion, the coarse grid ($N_y = 24$) solution, is convected in a stable manner, because it is conserved by the discrete convective operator. Therefore, we think that the symmetry-preserving discretization forms a solid basis for testing sub-grid scale models. The discrete convective operator transports energy from a resolved scale of motion to other resolved scales without dissipating any energy, as it should do from a physical point of view. The test for a sub-grid scale model then reads: does the addition of the dissipative sub-grid model to the conservative convection of the resolved scales reduce the error in the computation of u_{rms}.

The results for the fluctuating streamwise velocity u_{rms} are compared to the experimental data of Kreplin and Eckelmann [23] and to the numerical data of Kim et al. [20] as well as Gilbert and Kleiser [21] in Fig. 11. This comparison confirms that the fourth-order, symmetry-preserving method is more accurate than the second-order method. With 48 or more grid points in the wall normal direction, the root-mean-square of the fluctuating velocity obtained by the fourth-order method is in close agreement with that computed by Kim et al. [20] for $y^+ > 20$. In the vicinity of the wall ($y^+ < 20$), the velocity fluctuations of the fourth-order simulation method fit the experiment data nicely, even up to very coarse grids with only 24 grid points in the wall-normal direction. However, the turbulence intensity in the sub-layer ($0 < y^+ < 5$) predicted by the simulations is higher than that in the experiment. According to the fourth-order simulation the root-mean-square approaches the wall like $u_{\mathrm{rms}} \approx 0.38y^+$ ($N_y = 64$). The exact value of this slope is hard to pin-point experimentally. Hanratty et al. [26] have fitted experimental data of several investigators, and thus came to 0.3. Most direct numerical simulations yield higher values. Kim et al. [20] and Gilbert and Kleiser [21] have found slopes of 0.3637 and 0.3824 respectively, which is in close agreement with the present findings.

The normal component of the turbulent intensity is shown in Fig. 12. The results of all three computations are in good agreement. Yet, the computed level is lower than the measured level. Hence, either all computations (shown in Fig. 12) predict too low normal fluctuations, or the experiment of Kreplin and Eckelmann contains an error. Kim et al. [20] suppose that the latter may be the case as measurements of the normal component are extremely complicated close to a wall. As an example of this, Kim et al. refer to the comparison made by Finnicum and Hanratty [27], who have compared experimental results of the near-wall behavior of the fluctuating normal velocity. From that comparison (see Fig. 7 in [27]) Finnicum and Hanratty concluded that reliable near-wall experiments cannot be made with an X probe. Note that Kreplin and Eckelmann have used a X probe for the normal component, whereas the streamwise and spanwise data has been obtained with a V probe. The normal velocity should behave as y^{+2} from the wall to be compatible with the no-slip boundary condition and the continuity equation at the wall. In our simulation, as well as in that of Kim et al., this limiting wall behavior is only visible in a very small layer close to the wall. The present result indicates $v_{\mathrm{rms}} \approx 0.0075y^{+2}$ ($N_y = 64$), Kim et al. [20] reported $v_{\mathrm{rms}} \approx 0.009y^{+2}$, and Finnicum and Hanratty [27] estimated the limiting behavior as $v_{\mathrm{rms}} \approx 0.005y^{+2}$.

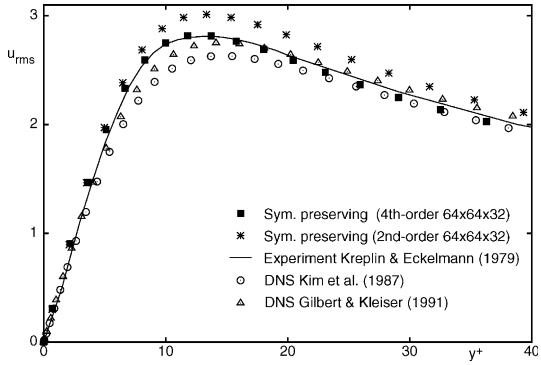

Fig. 11. Comparison of the mean-square of the fluctuating streamwise velocity as function of y^+.

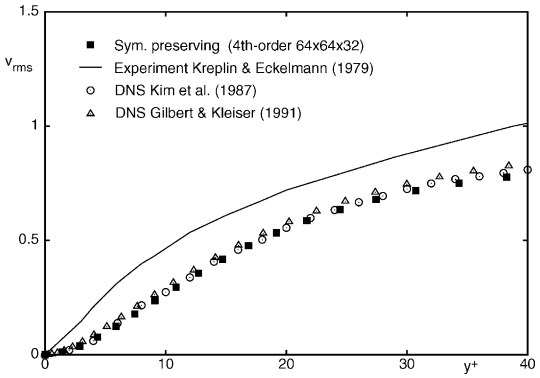

Fig. 12. Comparison of the mean-square of the fluctuating wall-normal velocity.

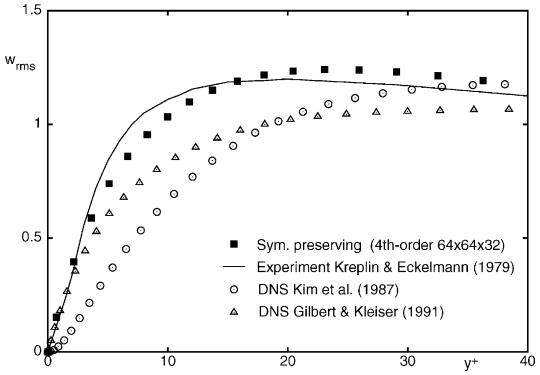

Fig. 13. Comparison of the mean-square of the fluctuating spanwise velocity.

Fig. 13 displays the spanwise component of the velocity fluctuations. As can be seen, the discrepancies among the computed results is noticeable larger for spanwise component than for the stream- and spanwise component. Especially the location of the maximum spanwise fluctuation varies fairly. Kim et al. [20] predict a maximum at $y^+ \approx 35$; the result of Gilbert and Kleiser [21] shows a broad plateau of maximum values for $20 < y^+ < 50$, whereas our computations reach the maximum at $y^+ \approx 22$, which is in close agreement with the experimental maximum at $y^+ \approx 20$.

So, in conclusion, the results of the fourth-order symmetry-preserving discretization agree better with the available reference data than those of its second-order counterpart, and with the fourth-order method a $64 \times 64 \times 32$ grid suffices to perform an accurate numerical simulation of a turbulent channel flow at $Re = 5600$ (where Reynolds number is based on channel width and bulk velocity).

5. Concluding remarks

The smallest scales of motion in a turbulent flow result from a subtle balance between convective transport and diffusive dissipation. In mathematical terms, the balance is an interplay between two differential operators differing in symmetry: the convective derivative is skew-symmetric, whereas diffusion is governed by a symmetric, positive-definite operator. With this in mind, we have developed a spatial dis-

cretization method which preserves the symmetries of the balancing differential operators. That is, convection is approximated by a skew-symmetric discrete operator, and diffusion is discretized by a symmetric, positive-definite operator. Second-order and fourth-order versions have been developed thus far, applicable to structured non-uniform grids. The resulting semi-discrete representation conserves mass, momentum and energy (in the absence of physical dissipation). As the coefficient matrices are stable and non-singular, a solution can be obtained on any grid, and the main question becomes how accurate is a symmetry-preserving discretization, or stated otherwise, how coarse may the grid be? This question has been addressed for a turbulent channel flow. The outcomes show that with the fourth-order method a $64 \times 64 \times 32$ grid suffices to perform an accurate numerical simulation of a turbulent channel flow at $Re = 5600$, where the Reynolds number is based on channel width and bulk velocity (which is equivalent to a Reynolds number of 180, based on the channel half-width and wall shear velocity).

Acknowledgements

The Stichting Nationale Computerfaciliteiten (National Computing Facilities Foundation, NCF) with financial support from the Netherlands Organization for Scientific Research (NWO) is gratefully acknowledged for the use of supercomputer facilities.

References

[1] R. Teman, Navier–Stokes Equations and Nonlinear Functional Analysis, CBMS-NSF regional conference series in applied mathematics, vol. 66, second ed., SIAM, 1995, p. 13.
[2] T.A. Manteufel, A.B. White Jr., The numerical solution of second-order boundary value problems on nonuniform meshes, Math. Comput. 47 (1986) 511.
[3] A.E.P. Veldman, K. Rinzema, Playing with nonuniform grids, J. Eng. Math. 26 (1991) 119.
[4] Y. Morinishi, T.S. Lund, O.V. Vasilyev, P. Moin, Fully conservative higher order finite difference schemes for incompressible flow, J. Comp. Phys. 143 (1998) 90.
[5] O.V. Vasilyev, High order finite difference schemes on non-uniform meshes with good conservation properties, J. Comp. Phys. 157 (2000) 746.
[6] F. Nicoud, Conservative high-order finite-difference schemes for low-Mach number flows, J. Comp. Phys. 158 (2000) 71.
[7] F. Ducros, F. Laporte, T. Soulères, V. Guinot, P. Moinat, B. Caruelle, High-order fluxes for conservative skew-symmetric-like schemes in structured meshes: application to compressible flows, J. Comp. Phys. 161 (2000) 114.
[8] A. Twerda, A.E.P. Veldman, S.W. de Leeuw, High order schemes for colocated grids: preliminary results. In: Proceedings of the 5th Annual Conference of the Advanced School for Computing and Imaging, 1999, p. 286.
[9] A. Twerda, Advanced computational methods for complex flow simulation, Ph.D. Thesis, Delft University of Technology, 2000.
[10] A. Jameson, W. Schmidt, E. Turkel, Numerical Solutions of the Euler Equations by Finite Volume Methods using Runge–Kutta Time Stepping, AIAA Paper 81-1259, 1981.
[11] D. Furihata, Finite difference schemes for $\frac{\partial u}{\partial t} = \left(\frac{\partial}{\partial x}\right)^{\alpha} \frac{\delta G}{\delta u}$ that inherit energy conservation or dissipation property, J. Comp. Phys. 156 (1999) 181.
[12] J.M. Hyman, R.J. Knapp, J.C. Scovel, High order finite volume approximations of differential operators on nonuniform grids, Phys. D 60 (1992) 112.
[13] J.E. Castillo, J.M. Hyman, M.J. Shaskov, S. Steinberg, The sensitivity and accuracy of fourth order finite-difference schems on nonuniform grids in one dimension, Comput. Math. Appl. 30 (1995) 41.
[14] J.M. Hyman, M. Shashkov, Natural discretizations for the divergence, gradient and curl on logically rectangular grids, Comput. Math. Appl. 33 (1997) 81.
[15] R.W.C.P. Verstappen, R.M. van der Velde, Symmetry-preserving discretization of heat transfer in a complex turbulent flow, submitted.
[16] R.W.C.P. Verstappen, A.E.P. Veldman, Direct numerical simulation of turbulence at lower costs, J. Eng. Math. 32 (1997) 143.
[17] R.W.C.P. Verstappen, A.E.P. Veldman, Spectro-consistent discretization of Navier–Stokes: a challenge to RANS and LES, J. Eng. Math. 34 (1998) 163.
[18] F.H. Harlow, J.E. Welsh, Numerical calculation of time-dependent viscous incompressible flow of fluid with free surface, Phys. Fluids 8 (1965) 2182.

[19] M. Antonopoulos-Domis, Large-eddy simulation of a passive scalar in isotropic turbulence, J. Fluid Mech. 104 (1981) 55–79.
[20] J. Kim, P. Moin, R. Moser, Turbulence statistics in fully developed channel flow at low Reynolds number, J. Fluid Mech. 177 (1987) 133.
[21] N. Gilbert, L. Kleiser, Turbulence model testing with the aid of direct numerical simulation results, in: Proceedings of the Turbulence Shear Flows 8, Paper 26-1, Munich, 1991.
[22] A. Kuroda, N. Kasagi, M. Hirata, Direct numerical simulation of turbulent plane Couette–Poisseuille flows: effect of mean shear rate on the near-wall turbulence structures, in: F. Durst, et al. (Eds.), Proc. Turb. Shear Flows, vol. 9, Springer, Berlin, 1995, pp. 241–257.
[23] H.P. Kreplin, H. Eckelmann, Behavior of the three fluctuating velocity components in the wall region of a turbulent channel flow, Phys. Fluids 22 (1979) 1233–1239.
[24] H. Eckelmann, The structure of the viscous sublayer and the adjacent wall region in a turbulent channel flow, J. Fluid Mech. 65 (1974) 439–459.
[25] R.B. Dean, Reynolds number dependence of skin friction and other bulk flow variables in two-dimensional rectangular duct flow, J. Fluids Eng. 100 (1978) 215–223.
[26] T.J. Hanratty, L.G. Chorn, D.T. Hatziavramidis, Turbulent fluctuations in the viscous wall region for Newtonian and drag reducing fluids, Phys. Fluids 20 (1977) S112.
[27] D.S. Finnicum, T.J. Hanratty, Turbulent normal velocity fluctuations close to a wall, Phys. Fluids 28 (1985) 1654–1658.